

Semileptonic decays of doubly charmed (bottom) baryons to single heavy baryons

M. Shekari Tousi^a and K. Azizi^{a,b*}

^a*Department of Physics, University of Tehran, North Kargar Avenue, Tehran 14395-547, Iran*

^b*Department of Physics, Dogus University, Dudullu-Ümraniye, 34775 Istanbul, Türkiye*

(Dated: April 25, 2025)

We investigate the semileptonic decays of baryons containing double charm or double bottom quarks, focusing on their transitions to single heavy baryons through three-point QCD sum rule framework. In our calculations, we take into account nonperturbative operators with mass dimensions up to five. We calculate the form factors associated with these decays, emphasizing the vector and axial-vector transition currents in the corresponding amplitude. By applying fitting functions for the form factors based on the squared momentum transfer, we derive predictions for decay widths and branching ratios in their possible lepton channels. These findings offer valuable insights for experimentalists exploring semileptonic decays of doubly charm or bottom baryons. Perhaps they can be validated in upcoming experiments like LHCb. These investigations contribute to a deeper understanding of the decay mechanisms in these baryonic channels.

I. INTRODUCTION

Since the quark model was introduced [1], efforts have been made to create a comprehensive hadron spectrum that includes all the particles predicted by the model. Recent studies focusing on hadrons with heavy quarks have attracted considerable interest. While the quark model has successfully explained many aspects of hadron spectra, it has yet to confirm all theoretically predicted particles, particularly the doubly heavy baryons. The first such baryon, the $\Xi_{cc}^+(3520)$, was identified by the SELEX collaboration in 2002 through its decay channel pD^+K^- [2], with a subsequent confirmation in 2005 [3]. In a landmark achievement, the LHCb experiment validated the existence of the doubly charm baryon $\Xi_{cc}^{++}(3621)$ in 2017, utilizing the decay channel $\Xi_{cc}^{++} \rightarrow \Lambda_c^+ K^- \pi^+ \pi^+$ [4], which was later confirmed in 2018 via $\Xi_{cc}^{++} \rightarrow \Xi_c^+ \pi^+$ [5]. In 2019, searches for the Ξ_{cc}^+ were conducted by LHCb through the decay $\Xi_{cc}^+ \rightarrow \Lambda_c^+ K^- \pi^+$ [6], and results from this investigation were integrated with findings from 2021 related to the decay $\Xi_{cc}^+ \rightarrow \Xi_c^+ \pi^- \pi^+$, achieving a maximum local significance of 4.0 standard deviations around 3620 MeV for the Ξ_{cc}^+ mass [7]. However, this does not signify a substantial gap between the masses of Ξ_{cc}^+ and Ξ_{cc}^{++} . Ongoing experimental efforts aim to uncover additional samples of these baryons, yet no new doubly heavy baryons have been discovered thus far [8]. Many scientists have engaged in extensive research to specify various properties of these type of baryons, including the masses and residues [9–29], chiral effective Lagrangians [30], strong coupling constants [31–37], strong interactions and decays [38–40], radiative decay [14, 19, 29, 33, 41, 42], weak decay processes [43–68], magnetic moments [69, 70], lifetimes [71], mixing angles [72], etc., employing diverse methodologies. To accurately compute these characteristics, nonperturbative techniques such as QCD sum rules, introduced by Shifman, Vainshtein, and Zakharov in 1979 [73, 74], are essential. This approach is based on the QCD Lagrangian utilizing correlation function through various interpolating currents. This method has made numerous successful predictions regarding hadronic parameters, validated by various experiments, and is considered highly effective [10, 75–79].

In this research, we discuss weak decays of the doubly heavy spin-1/2 baryons Ξ_{cc}^{++} , Ξ_{cc}^+ , Ω_{cc}^+ , Ξ_{bb}^0 , Ξ_{bb}^- and Ω_{bb}^- , specifically focusing on their transitions to spin-1/2 single heavy baryons. At the quark level, these decays occur through $c \rightarrow d/s$ or $b \rightarrow u/c$ transitions, with the two spectator quarks. The $b \rightarrow c$ transition will not be addressed in this work and will be reserved for future study. We begin by deriving the form factors for these transitions using three-point QCD sum rule method. We then utilize these form factors to estimate the decay widths and branching ratios for semileptonic processes of doubly heavy baryons. Our findings indicate that these decay channels are significant and could be investigated in future experiments such as LHCb.

Previous research has explored transitions through various methodologies, including the QCD sum rule approach with different interpolating currents [64] and the light-front framework [48], considering the two leptons, e and μ the same. In this work, we calculate the pertinent form factors by utilizing a comprehensive set of interpolating currents applicable to both initial and final baryonic states, building upon recently established residues and masses for doubly heavy baryons [9]. Our analysis includes a detailed examination of decay widths and branching ratios

*Electronic address: kazem.azizi@ut.ac.ir; Corresponding author

across all possible lepton channels. By meticulously optimizing critical parameters, such as the mixing parameter in the interpolating currents, we aim to enhance the precision of our results while minimizing uncertainties.

This paper is organized as follows: In Section II, we derive the sum rules that govern the form factors relevant to the semileptonic decay of doubly heavy baryons. Section III focuses on the numerical evaluation of these sum rules, showcasing fit functions that reveal how the form factors vary with respect to the squared momentum transfer. In Section IV, we present our findings on decay widths and branching ratios across all possible lepton channels. Lastly, Section V wraps up the discussion, and further calculation details can be found in the Appendix.

II. EVALUATION OF FORM FACTORS VIA QCD SUM RULE METHOD

Before delving into the detailed calculations of sum rules to evaluate the weak decay form factors of doubly heavy baryons, we first investigate the ground states of these baryons within the quark model. In the ground state of doubly heavy baryons featuring identical heavy quarks, denoted as $\Xi_{QQ}^{(*)}$ and $\Omega_{QQ}^{(*)}$, the two heavy quarks combine to form a diquark with a total spin of 1. When we include the spin-1/2 of the light quark, we can have states with either total spin-1/2 or spin-3/2. Baryons with a star represent the spin-3/2 states, while those without represent the spin-1/2 states. For these configurations, the interpolating current must be symmetric in relation to the exchange of the heavy quark fields. For baryons comprising two different heavy quarks, in addition to the spin-1 diquark case, the diquark can also have a total spin of zero, resulting in overall spin-1/2 states. In these cases, the interpolating currents, typically labeled as Ξ'_{bc} and Ω'_{bc} , are antisymmetric with respect to the two heavy quark fields. This work focuses exclusively on spin-1/2 doubly heavy baryons. With those initial points in mind, let's return to our central issue. We investigate the weak decays of the the doubly heavy baryons considering the following semileptonic decay channels:

- The cc sector:

$$\begin{aligned}\Xi_{cc}^{++}(ccu) &\rightarrow \Lambda_c^+(dcu)/\Sigma_c^+(dcu)/\Xi_c^+(scu)/\Xi_c'^+(scu), \\ \Xi_{cc}^+(ccd) &\rightarrow \Sigma_c^0(dcd)/\Xi_c^0(scd)/\Xi_c'^0(scd), \\ \Omega_{cc}^+(ccs) &\rightarrow \Xi_c^0(dcs)/\Xi_c'^0(dcs)/\Omega_c^0(scs),\end{aligned}$$

- The bb sector:

$$\begin{aligned}\Xi_{bb}^0(bbu) &\rightarrow \Sigma_b^+(ubu), \\ \Xi_{bb}^-(bbd) &\rightarrow \Lambda_b^0(ubd)/\Sigma_b^0(ubd), \\ \Omega_{bb}^-(bbs) &\rightarrow \Xi_b^0(ubs)/\Xi_b'^0(ubs).\end{aligned}$$

In these categories, the quark components are clearly indicated in brackets, with the first quarks representing those involved in the decays. Although in our previous study [46], we performed calculations of the decay of $\Xi_{cc}^{++} \rightarrow \Xi_c^+ \bar{\ell} \nu_\ell$ in two possible lepton channels (e^+ and μ^+), in this study we investigate the remaining semileptonic decay channels. Among the different types of doubly charm baryons, three can decay via weak interactions: the Ξ_{cc} isodoublet (ccu , ccd) and the Ω_{cc} isosinglet (ccs) shown in Fig. 1. Similarly, there are three corresponding doubly bottom baryons. In the decay final state of the Ξ_{cc} and Ω_{cc} , we observe baryons that each contain one charm quark. These baryons are organized into antitriplets and sextets of charm baryons, illustrated in Fig. 2. A similar structure exists for baryons with one bottom quark. The baryons depicted in Fig. 2 possess a total spin of 1/2, while another sextet exhibits a spin of 3/2. This study will concentrate on the $1/2 \rightarrow 1/2$ transition.

To calculate these decay channels, we use the QCD sum rules that utilize a systematic method to evaluate a correlation function via two distinct approaches. The first, known as the physical or phenomenological side, incorporates hadronic degrees of freedom and yields results related to physical quantities like the masses and residues of hadronic states. The second side, known as the QCD or OPE side, utilizes the fundamental principles of quantum chromodynamics. This includes aspects such as coupling constants, quark-gluon condensates, and the masses of quarks. By matching conclusions from both sides and concentrating on the coefficients associated with corresponding Lorentz structures, we can establish QCD sum rules for the relevant physical properties.

A. Physical approach

The considered semileptonic transitions occur via $c \rightarrow d/s \bar{\ell} \nu_\ell$ and $b \rightarrow u \ell \bar{\nu}_\ell$ transitions (see Fig. 3):

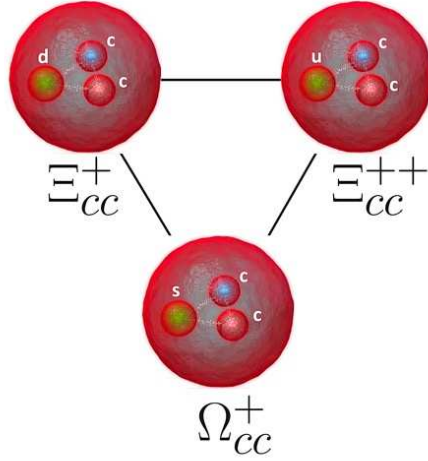


FIG. 1: Doubly charm baryons with spin-1/2. The case is similar for the doubly bottom baryons and those containing bottom and charm quarks.

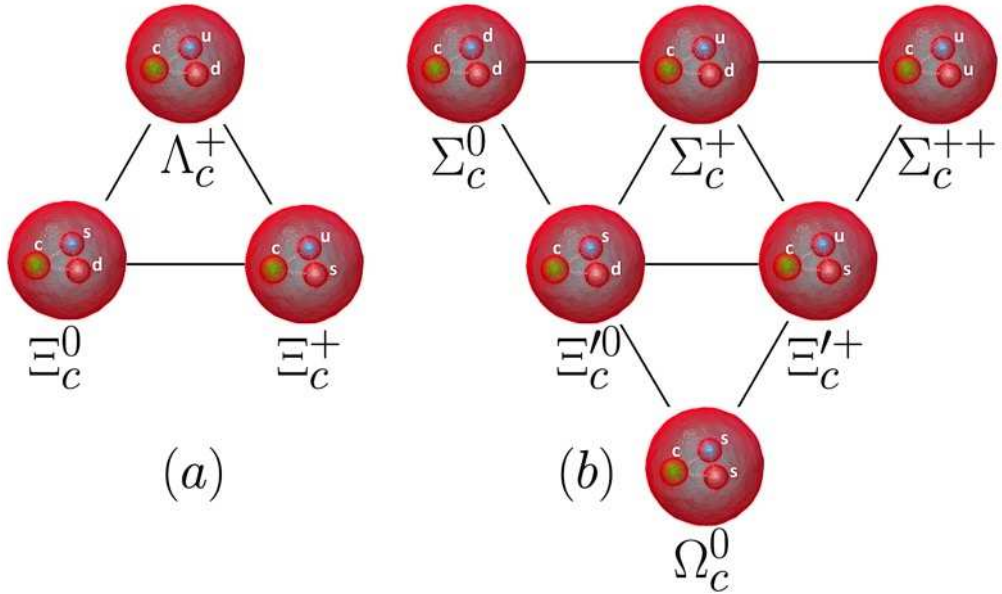


FIG. 2: Antitriplets (Panel a) and Sextets (Panel b) of single charm baryons featuring one charm quark and two light quarks. The pattern is similar for the baryons containing a bottom quark. These baryons have a total spin of 1/2, while other sextet exhibiting spin 3/2 are not shown in the figure.

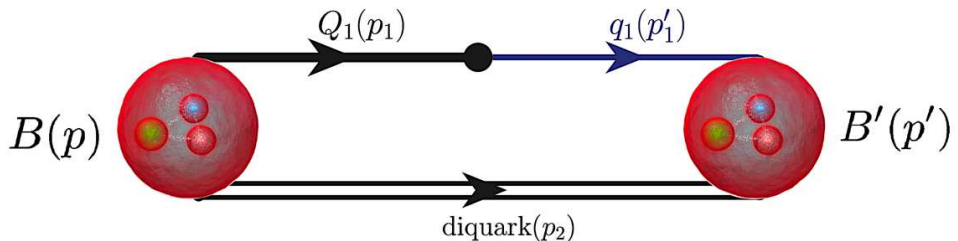


FIG. 3: Feynman diagram depicting the decay of doubly heavy baryons B into a single heavy baryons B' , with two spectator quarks forming a diquark. The momentum of the initial and final baryons are represented as p and p' respectively. At the quark level, a heavy quark Q_1 transits into a light quark q_1 , and we have two spectator quarks. The black circle symbolizes the weak interaction vertex.

To evaluate the transition amplitude, we require the low-energy effective Hamiltonian calculated at the quark level. The effective Hamiltonian for these semileptonic processes can be written as:

$$\begin{aligned}\mathcal{H}_{\text{eff}} &= \frac{G_F}{\sqrt{2}} V_{cs}^* [\bar{s} \gamma_\mu (1 - \gamma_5) c] [\bar{\nu}_\ell \gamma^\mu (1 - \gamma_5) l], \\ \mathcal{H}_{\text{eff}} &= \frac{G_F}{\sqrt{2}} V_{cd}^* [\bar{d} \gamma_\mu (1 - \gamma_5) c] [\bar{\nu}_\ell \gamma^\mu (1 - \gamma_5) l], \\ \text{or} \\ \mathcal{H}_{\text{eff}} &= \frac{G_F}{\sqrt{2}} V_{ub}^* [\bar{u} \gamma_\mu (1 - \gamma_5) b] [\bar{l} \gamma^\mu (1 - \gamma_5) \nu_\ell],\end{aligned}\quad (1)$$

where the elements $V_{cs,cd,ub}$ are associated with the Cabibbo-Kobayashi-Maskawa (CKM) matrix and the Fermi coupling constant, referred to as G_F . The decay amplitude is derived by sandwiching the effective Hamiltonian between the states of the initial and final baryons. These decay processes incorporate both the vector (V_μ) and axial vector (A_μ) transitions, each characterized by three form factors. The parameterizations of these transitions are crafted to uphold Lorentz invariance and respect parity constraints, as outlined in [80]:

$$\begin{aligned}\langle B'(p', s') | V^\mu | B(p, s) \rangle &= \bar{u}_{B'}(p', s') \left[F_1(q^2) \gamma^\mu + F_2(q^2) \frac{p'^\mu}{m_B} + F_3(q^2) \frac{p'^\mu}{m_{B'}} \right] u_B(p, s), \\ \langle B'(p', s') | A^\mu | B(p, s) \rangle &= \bar{u}_{B'}(p', s') \left[G_1(q^2) \gamma^\mu + G_2(q^2) \frac{p^\mu}{m_B} + G_3(q^2) \frac{p^\mu}{m_{B'}} \right] \gamma_5 u_B(p, s),\end{aligned}\quad (2)$$

where $F_1(q^2)$, $F_2(q^2)$, and $F_3(q^2)$ represent the form factors associated with the vector transition, while $G_1(q^2)$, $G_2(q^2)$, and $G_3(q^2)$ correspond to the form factors of the axial transition. The Dirac spinors for the initial and final baryon states are denoted as $u_B(p, s)$ and $u_{B'}(p', s')$ respectively, and the transferred momentum of the leptons is given by $q = p - p'$. To compute the form factors, we will employ the three-point correlation function:

$$\Pi_\mu(p, p', q) = i^2 \int d^4x e^{-ip \cdot x} \int d^4y e^{ip' \cdot y} \langle 0 | \mathcal{T} \{ \mathcal{J}^{B'}(y) \mathcal{J}_\mu^{tr,V(A)}(0) \bar{\mathcal{J}}^B(x) \} | 0 \rangle, \quad (3)$$

where we denote the interpolating currents of the initial and final baryons as $\mathcal{J}^B(x)$ and $\mathcal{J}^{B'}(y)$, respectively, while \mathcal{T} represents the time-ordering operator. To compute the correlation function of the physical side, we must insert two appropriate complete sets of hadronic states that share the same quantum numbers as the currents $\mathcal{J}^B(x)$ and $\mathcal{J}^{B'}(y)$ at the relevant positions. Through a series of algebraic manipulations, we can express the physical side of the correlation function as follows:

$$\Pi_\mu^{Phys.}(p, p', q) = \frac{\langle 0 | \mathcal{J}^{B'}(0) | B'(p') \rangle \langle B'(p') | \mathcal{J}_\mu^{tr,V(A)}(0) | B(p) \rangle \langle B(p) | \bar{\mathcal{J}}^B(0) | 0 \rangle}{(p'^2 - m_{B'}^2)(p^2 - m_B^2)} + \dots, \quad (4)$$

where \dots denotes the continuum and higher states. Additionally, we describe the residues for the initial baryons (λ_B) and the final baryons ($\lambda_{B'}$) as follows:

$$\begin{aligned}\langle 0 | \mathcal{J}^{B'}(0) | B'(p') \rangle &= \lambda_{B'} u_{B'}(p', s'), \\ \langle B(p) | \bar{\mathcal{J}}^B(0) | 0 \rangle &= \lambda_B^+ \bar{u}_B(p, s).\end{aligned}\quad (5)$$

After performing the summations on Dirac spinors:

$$\begin{aligned}\sum_{s'} u_{B'}(p', s') \bar{u}_{B'}(p', s') &= \not{p}' + m_{B'}, \\ \sum_s u_B(p, s) \bar{u}_B(p, s) &= \not{p} + m_B,\end{aligned}\quad (6)$$

we achieve a definition for the physical side. In the following, we utilize the double Borel transformation [81]:

$$\hat{\mathbf{B}} \frac{1}{(p^2 - s)^m} \frac{1}{(p'^2 - s')^n} \longrightarrow (-1)^{m+n} \frac{1}{\Gamma[m]\Gamma[n]} \frac{1}{(M^2)^{m-1}} \frac{1}{(M'^2)^{n-1}} e^{-s/M^2} e^{-s'/M'^2}, \quad (7)$$

where we define the Borel mass parameters M^2 and M'^2 , which will be detailed in the subsequent numerical evaluations. The Borel transformation serves to suppress the influence of excited states and continuum contributions, thereby amplifying the ground state effects in both the initial and final states. After implementing the double Borel transformation, we obtain:

$$\begin{aligned} \hat{\mathbf{B}} \Pi_{\mu}^{\text{Phys.}}(p, p', q) = & \lambda_B \lambda_{B'} e^{-\frac{m_B^2}{M^2}} e^{-\frac{m_{B'}^2}{M'^2}} \left[F_1 \left(m_B m_{B'} \gamma_\mu + m_B \not{p}' \gamma_\mu + m_{B'} \gamma_\mu \not{p} + \not{p}' \gamma_\mu \not{p} \right) + \right. \\ & F_2 \left(\frac{m_{B'}}{m_B} p_\mu \not{p} + \frac{1}{m_B} p_\mu \not{p}' \not{p} + m_{B'} p_\mu + p_\mu \not{p}' \right) + F_3 \left(\frac{1}{m_{B'}} p'_\mu \not{p}' \not{p} + p'_\mu \not{p}' + p'_\mu \not{p} + m_{B'} p'_\mu \right) - \\ & G_1 \left(m_B m_{B'} \gamma_\mu \gamma_5 + m_B \not{p}' \gamma_\mu \gamma_5 - m_{B'} \gamma_\mu \not{p} \gamma_5 - \not{p}' \gamma_\mu \not{p} \gamma_5 \right) - G_2 \left(p_\mu \not{p}' \gamma_5 + m_{B'} p_\mu \gamma_5 - \frac{m_{B'}}{m_B} p_\mu \not{p} \gamma_5 - \frac{1}{m_B} p_\mu \not{p}' \not{p} \gamma_5 \right) \\ & \left. - G_3 \left(\frac{m_B}{m_{B'}} p'_\mu \not{p}' \gamma_5 + m_{B'} p'_\mu \gamma_5 - \frac{1}{m_{B'}} p'_\mu \not{p}' \not{p} \gamma_5 - p'_\mu \not{p} \gamma_5 \right) \right] + \dots . \end{aligned} \quad (8)$$

B. QCD approach

To develop the QCD or OPE approach, we must evaluate the correlation function presented in Eq. (3) by incorporating the appropriate interpolating currents for the initial and final baryon states. This process involves utilizing the interpolating currents specifically designed for sextet and antitriplet single heavy baryons with spin-parity $J^P = (\frac{1}{2})^+$, as outlined in [82]:

$$\mathcal{J}_{B'}^{(s)} = -\frac{1}{\sqrt{2}} \epsilon^{abc} \left\{ \left(q_1^{aT} C Q^b \right) \gamma_5 q_2^c + \beta \left(q_1^{aT} C \gamma_5 Q^b \right) q_2^c - \left[\left(Q^{aT} C q_2^b \right) \gamma_5 q_1^c + \beta \left(Q^{aT} C \gamma_5 q_2^b \right) q_1^c \right] \right\}, \quad (9)$$

$$\begin{aligned} \mathcal{J}_{B'}^{(anti-t)} = & \frac{1}{\sqrt{6}} \epsilon^{abc} \left\{ 2 \left(q_1^{aT} C q_2^b \right) \gamma_5 Q^c + 2\beta \left(q_1^{aT} C \gamma_5 q_2^b \right) Q^c + \left(q_1^{aT} C Q^b \right) \gamma_5 q_2^c + \beta \left(q_1^{aT} C \gamma_5 Q^b \right) q_2^c \right. \\ & \left. + \left(Q^{aT} C q_2^b \right) \gamma_5 q_1^c + \beta \left(Q^{aT} C \gamma_5 q_2^b \right) q_1^c \right\}, \end{aligned} \quad (10)$$

and we utilize the interpolating currents for doubly charm (bottom) baryons with spin-parity $J^P = (\frac{1}{2})^+$ as follow [10]:

$$\mathcal{J}_B^{(s)}(x) = \sqrt{2} \epsilon_{abc} \left\{ \left(Q^{aT}(x) C q^b(x) \right) \gamma_5 Q^c(x) + \beta \left(Q^{aT}(x) C \gamma_5 q^b(x) \right) Q^c(x) \right\}, \quad (11)$$

where the indices a, b , and c represent color values, while C denotes the charge conjugation operator. The symbols Q and q indicate heavy and light quark fields, respectively. We introduce a parameter β , which will be determined through numerical analysis; specifically, the value $\beta = -1$ aligns with the Ioffe current. Our approach to calculating the QCD side begins with the inclusion of the interpolating currents associated with the initial and final baryons, as well as the transition current, into the correlation function. Utilizing Wick's theorem, we carry out all possible contractions involving the quark fields, enabling us to reformulate the correlation function in terms of the propagators for both the heavy and light quark components.

We evaluate this calculation for all decay channels described earlier in this context and present the results for all decay channels, but as an example, we only show the calculations for the semileptonic transition $\Omega_b^- \rightarrow \Xi_b^0 \ell \bar{\nu}_\ell$. The final result, in this step, for this decay channel is:

$$\begin{aligned} \Pi_{\mu}^{OPE} = & i^2 \int d^4 x e^{-ipx} \int d^4 y e^{ip'y} \frac{1}{\sqrt{3}} \epsilon_{a'b'c'} \epsilon_{abc} \left\{ 2\gamma_5 S_b^{ca'}(y-x) S_u'^{ab'}(y-x) S_s'^{bi}(y) \gamma_\mu (1-\gamma_5) S_b^{ic'}(-x) \gamma_5 \right. \\ & + 2Tr[S_u'^{ab'}(y-x) S_b'^{ia'}(-x) (1-\gamma_5) \gamma_\mu S_s'^{bi}(y)] \gamma_5 S_b'^{cc'}(y-x) \gamma_5 - 2\beta Tr[S_s'^{bi}(y) \gamma_\mu (1-\gamma_5) S_b'^{ia'}(-x) \gamma_5 S_u'^{ab'}(y-x)] \\ & \left. \gamma_5 S_b'^{cc'}(y-x) + 2\beta \gamma_5 S_b'^{ca'}(y-x) \gamma_5 S_u'^{ab'}(y-x) S_s'^{bi}(y) \gamma_\mu (1-\gamma_5) S_b'^{ic'}(-x) - Tr[S_b'^{ba'}(y-x) S_u'^{ab'}(y-x)] \gamma_5 S_s'^{ci}(y) \right\} \end{aligned}$$

$$\begin{aligned}
& \gamma_\mu(1 - \gamma_5)S_b^{ic'}(-x)\gamma_5 + \gamma_5 S_s^{ci}(y)\gamma_\mu(1 - \gamma_5)S_b'^{ab'}(-x)\gamma_5S_u'^{ab'}(y-x)S_b^{bc'}(y-x) - \beta\gamma_5S_s^{ci}(y)\gamma_\mu(1 - \gamma_5)S_b^{ic'}(-x) \\
& Tr[\gamma_5S_b'^{ba'}(y-x)S_u'^{ab'}(y-x)] + \beta\gamma_5S_s^{ci}(y)\gamma_\mu(1 - \gamma_5)S_b'^{ab'}(-x)\gamma_5S_u'^{ab'}(y-x)S_b^{bc'}(y-x) + \gamma_5S_u'^{cb'}(y-x)S_b'^{aa'}(y-x) \\
& S_s^{bi}(y)\gamma_\mu(1 - \gamma_5)S_b'^{ic'}(-x)\gamma_5 + \gamma_5S_u'^{cb'}(y-x)S_b'^{ia'}(-x)(1 - \gamma_5)\gamma_\mu S_s'^{bi}(y)S_b'^{ac'}(y-x)\gamma_5 + \beta\gamma_5S_u'^{cb'}(y-x)\gamma_5S_b'^{aa'}(y-x) \\
& S_s^{bi}(y)\gamma_\mu(1 - \gamma_5)S_b'^{ic'}(-x) + \beta\gamma_5S_u'^{cb'}(y-x)\gamma_5S_b'^{ia'}(-x)(1 - \gamma_5)\gamma_\mu S_s'^{bi}(y)S_b'^{ac'}(y-x) - 2\beta Tr[S_u'^{ab'}(y-x)\gamma_5S_s^{bi}(y)\gamma_\mu \\
& (1 - \gamma_5)S_b'^{ia'}(-x)]S_b'^{cc'}(y-x)\gamma_5 + 2\beta Tr[S_b'^{ba'}(y-x)\gamma_5S_u'^{ab'}(y-x)]S_s^{bi}(y)\gamma_\mu(1 - \gamma_5)S_b^{ic'}(-x)\gamma_5 + 2\beta^2S_b'^{ca'}(y-x)\gamma_5 \\
& S_u'^{ab'}(y-x)\gamma_5S_s^{bi}(y)\gamma_\mu(1 - \gamma_5)S_b^{ic'}(-x) - 2\beta^2 Tr[S_u'^{ab'}(y-x)\gamma_5S_b'^{ia'}(-x)(1 - \gamma_5)\gamma_\mu S_s'^{bi}(y)\gamma_5]S_b'^{cc'}(y-x) \\
& - 2\beta Tr[S_u'^{ab'}(y-x)\gamma_5S_b'^{ba'}(y-x)\gamma_5]S_s^{ci}(y)\gamma_\mu(1 - \gamma_5)S_b^{ic'}(-x)\gamma_5 - \beta S_s^{ci}(y)\gamma_\mu(1 - \gamma_5)S_b'^{ia'}(-x)S_u'^{ab'}(y)\gamma_5S_b'^{bc'}(y-x)\gamma_5 \\
& S_b'^{bc'}(y-x) + \beta S_u'^{cb'}(y-x)S_b'^{aa'}(y-x)\gamma_5S_s^{bi}(y)\gamma_\mu(1 - \gamma_5)S_b'^{ic'}(-x)\gamma_5 + \beta S_u'^{cb'}(y-x)S_b'^{ia'}(-x)(1 - \gamma_5)\gamma_\mu S_s'^{bi}(y)\gamma_5 \\
& S_b'^{ac'}(y-x)\gamma_5 + \beta^2 S_u'^{cb'}(y-x)\gamma_5S_b'^{ia'}(-x)(1 - \gamma_5)\gamma_\mu S_s'^{bi}(y)\gamma_5S_b'^{ac'}(y-x) + \beta^2 S_u'^{cb'}(y-x)\gamma_5S_b'^{aa'}(y-x)\gamma_5S_s^{bi}(y) \\
& \gamma_\mu(1 - \gamma_5)S_b^{ic'}(-x) \Big\}, \tag{12}
\end{aligned}$$

where $S' = CS^TC$. We use the expression of the light and heavy quark propagators [83]:

$$\begin{aligned}
S_q^{ab}(x) &= i\delta_{ab}\frac{\not{x}}{2\pi^2x^4} - \delta_{ab}\frac{m_q}{4\pi^2x^2} - \delta_{ab}\frac{\langle\bar{q}q\rangle}{12} + i\delta_{ab}\frac{\not{x}m_q\langle\bar{q}q\rangle}{48} - \delta_{ab}\frac{x^2}{192}\langle\bar{q}g\sigma Gq\rangle + i\delta_{ab}\frac{x^2\not{x}m_q}{1152}\langle\bar{q}g\sigma Gq\rangle \\
&- i\frac{gG_{ab}^{\alpha\beta}}{32\pi^2x^2}[\not{x}\sigma_{\alpha\beta} + \sigma_{\alpha\beta}\not{x}] - i\delta_{ab}\frac{x^2\not{x}g^2\langle\bar{q}q\rangle^2}{7776} - \delta_{ab}\frac{x^4\langle\bar{q}q\rangle\langle g^2G^2\rangle}{27648} + \dots, \tag{13}
\end{aligned}$$

and

$$\begin{aligned}
S_Q^{ab}(x) &= i\int\frac{d^4k}{(2\pi)^4}e^{-ikx}\left\{\frac{\delta_{ab}(\not{k}+m_Q)}{k^2-m_Q^2} - \frac{gG_{ab}^{\mu\nu}}{4}\frac{\sigma_{\mu\nu}(\not{k}+m_Q)+(\not{k}+m_Q)\sigma_{\mu\nu}}{(k^2-m_Q^2)^2} + \frac{g^2G^2}{12}\delta_{ab}m_Q\frac{k^2+m_Q\not{k}}{(k^2-m_Q^2)^4}\right. \\
&\left.+ \dots\right\}, \tag{14}
\end{aligned}$$

where $G_{\mu\nu}$ represents the gluon field strength tensor, with $G_{\mu\nu}^{ab} = G_A^{\mu\nu}t_A^{ab}$, and $t_A = \frac{\lambda_A}{2}$ and $G^2 = G_A^{\mu\nu}G_{A\mu\nu}$. The indices A range from 1 to 8, corresponding to the Gell-Mann matrices. In the realm of QCD, we analyze the three-points correlation function within the deep Euclidean region using the OPE. Employing Wilson's OPE framework, we observe that the contributions from light and heavy quark propagators involve operators characterized by distinct mass dimensions. The bare-loop term, which has a mass dimension of $d = 0$, results in a perturbative impact. In contrast, nonperturbative corrections emerge from operators with varying dimensions, such as $d = 3$ for the quark condensate $\langle\bar{q}q\rangle$, $d = 4$ represented by $\langle G^2 \rangle$, and $d = 5$ exemplified by $\langle q\sigma G\bar{q} \rangle$. After we substitute the quark propagators into the correlation function, the resulting terms are expressed as follows:

$$\int d^4k \int d^4k' \int d^4xe^{i(k+k'-p).x} \int d^4ye^{i(-k'+p').y} \frac{1}{(k^2-m_Q^2)^l(k'^2-m_{Q'}^2)^f[y^2]^n[(y-x)^2]^m}. \tag{15}$$

Using the identity below, $(y-x)$ and y appear in the exponential form [84]:

$$\frac{1}{[(y)^2]^n} = \int \frac{d^D t}{(2\pi)^D} e^{-it\cdot(y)} i (-1)^{n+1} 2^{D-2n} \pi^{D/2} \frac{\Gamma(D/2-n)}{\Gamma(n)} \left(-\frac{1}{t^2}\right)^{D/2-n}, \tag{16}$$

and

$$\frac{1}{[(y-x)^2]^m} = \int \frac{d^D t'}{(2\pi)^D} e^{-it'\cdot(y-x)} i (-1)^{m+1} 2^{D-2m} \pi^{D/2} \frac{\Gamma(D/2-m)}{\Gamma(m)} \left(-\frac{1}{t'^2}\right)^{D/2-m}. \tag{17}$$

By placement $x_\mu \rightarrow i\frac{\partial}{\partial p_\mu}$ and $y_\mu \rightarrow -i\frac{\partial}{\partial p'_\mu}$, we get for instance:

$$\int d^4k \int d^4k' \int d^4xe^{i(k+k'-p+t').x} \int d^4ye^{i(-k'+p'-t-t').y} \int d^D t' \int d^D t$$

$$\frac{1}{(k^2 - m_Q^2)^l (k'^2 - m_{Q'}^2)^f} \left(-\frac{1}{t^2} \right)^{D/2-n} \left(-\frac{1}{t'^2} \right)^{D/2-m}, \quad (18)$$

and after performing the Fourier integrals, we have:

$$\int d^4x e^{i(k+k'-p+t').x} = (2\pi)^4 \delta^4(k + k' - p + t'), \quad (19)$$

and

$$\int d^4y e^{i(-k'+p'-t-t').y} = (2\pi)^4 \delta^4(-k' + p' - t - t'). \quad (20)$$

The Dirac delta functions simplify the expression by eliminating the integrals over k and k' . To solve the remaining integrals, we use the Feynman parameterization:

$$\frac{1}{A_1^{\alpha_1} A_2^{\alpha_2} A_3^{\alpha_3} A_4^{\alpha_4}} = \frac{\Gamma(\alpha_1 + \alpha_2 + \alpha_3 + \alpha_4)}{\Gamma(\alpha_1)\Gamma(\alpha_2)\Gamma(\alpha_3)\Gamma(\alpha_4)} \int_0^1 \int_0^{1-r} \int_0^{1-r-z} dz dr db \\ \frac{r^{\alpha_1-1} z^{\alpha_2-1} b^{\alpha_3-1} (1-r-z-b)^{\alpha_4-1}}{[rA_1 + zA_2 + bA_3 + (1-r-z-b)A_4]^{\alpha_1+\alpha_2+\alpha_3+\alpha_4}}. \quad (21)$$

In the final step, we use the following identity to extract the imaginary parts [84]:

$$\Gamma[\frac{D}{2} - n](-\frac{1}{L})^{D/2-n} = \frac{(-1)^{n-1}}{(n-2)!} (-L)^{n-2} \ln[-L]. \quad (22)$$

By evaluating the correlation function, we take into account perturbative contribution and nonperturbative operators with mass dimensions up to five. For the purposes of this study, we assume the masses of the light quarks are zero. Comparing the results from theoretical predictions and experiments data shows that the effect of this approximation is minimal in many studies. Upon integrating, we express the correlation function in terms of 24 distinct Lorentz structures as presented below:

$$\Pi_\mu^{\text{OPE}}(p, p', q) = \Pi_{p'\gamma_\mu p}^{\text{OPE}}(p^2, p'^2, q^2) p'\gamma_\mu p + \Pi_{p_\mu p' p}^{\text{OPE}}(p^2, p'^2, q^2) p_\mu p' p + \Pi_{p'_\mu p' p}^{\text{OPE}}(p^2, p'^2, q^2) p'_\mu p' p + \Pi_{p'_\mu p' \gamma_5}^{\text{OPE}}(p^2, p'^2, q^2) p'_\mu p' \gamma_5 + \Pi_{p'_\mu p' p \gamma_5}^{\text{OPE}}(p^2, p'^2, q^2) p'_\mu p' p \gamma_5 + \Pi_{p'\gamma_\mu \gamma_5}^{\text{OPE}}(p^2, p'^2, q^2) p'\gamma_\mu \gamma_5 + \Pi_{p'\gamma_\mu p \gamma_5}^{\text{OPE}}(p^2, p'^2, q^2) p'\gamma_\mu p \gamma_5 + \Pi_{p_\mu p' \gamma_5}^{\text{OPE}}(p^2, p'^2, q^2) p_\mu p' \gamma_5 + \Pi_{p'_\mu p' \gamma_5}^{\text{OPE}}(p^2, p'^2, q^2) p'_\mu p' \gamma_5 + \Pi_{p_\mu p' \gamma_5}^{\text{OPE}}(p^2, p'^2, q^2) p_\mu p' \gamma_5 + \Pi_{p'_\mu \gamma_5}^{\text{OPE}}(p^2, p'^2, q^2) p'_\mu \gamma_5 + \Pi_{p'_\mu p \gamma_5}^{\text{OPE}}(p^2, p'^2, q^2) p'_\mu p \gamma_5 + \Pi_{p_\mu p \gamma_5}^{\text{OPE}}(p^2, p'^2, q^2) p_\mu p \gamma_5 + \Pi_{p_\mu \gamma_5}^{\text{OPE}}(p^2, p'^2, q^2) p_\mu \gamma_5 + \Pi_{p'_\mu \gamma_5}^{\text{OPE}}(p^2, p'^2, q^2) p'_\mu \gamma_5 + \Pi_{p'_\mu p \gamma_5}^{\text{OPE}}(p^2, p'^2, q^2) p'_\mu p \gamma_5 + \Pi_{p_\mu p \gamma_5}^{\text{OPE}}(p^2, p'^2, q^2) p_\mu p \gamma_5 + \Pi_{p_\mu \gamma_5}^{\text{OPE}}(p^2, p'^2, q^2) p_\mu \gamma_5. \quad (23)$$

The invariant functions $\Pi_i^{\text{OPE}}(p^2, p'^2, q^2)$ (where i indicates different structures) are characterized using double dispersion integrals:

$$\Pi_i^{\text{OPE}}(p^2, p'^2, q^2) = \int_{s_{min}}^{\infty} ds \int_{s'_{min}}^{\infty} ds' \frac{\rho_i^{\text{OPE}}(s, s', q^2)}{(s-p^2)(s'-p'^2)}, \quad (24)$$

where $s_{min} = (m_Q + m_{Q'})^2$, $s'_{min} = m_Q^2$ and $\rho_i^{\text{OPE}}(s, s', q^2)$ represent the spectral densities, given by $\rho_i^{\text{OPE}}(s, s', q^2) = \frac{1}{\pi} \text{Im} \Pi_i^{\text{OPE}}(p^2, p'^2, q^2)$. By employing the quark-hadron duality assumption, the upper limits of the integrals are changed to s_0 and s'_0 , which denote the continuum thresholds for the initial and final baryon states. The spectral densities can be expressed as follows:

$$\rho_i^{\text{OPE}}(s, s', q^2) = \rho_i^{\text{Pert.}}(s, s', q^2) + \sum_{n=3}^5 \rho_i^n(s, s', q^2). \quad (25)$$

In this study, we denote the perturbative component of our calculations as $\rho_i^{\text{Pert.}}(s, s', q^2)$ and the summation $\sum_{n=3}^5 \rho_i^n(s, s', q^2)$ that captures all mass dimensions relevant to the nonperturbative aspects of our analysis. This

includes contributions from the quark condensate, gluon condensate, and the mixed quark-gluon condensate. Additionally, we implement a double Borel transformation on the QCD side and conduct a continuum subtraction. As a result, we have:

$$\Pi_i^{\text{OPE}}(M^2, M'^2, s_0, s'_0, q^2) = \int_{s_{\min}}^{s_0} ds \int_{s'_{\min}}^{s'_0} ds' e^{-s/M^2} e^{-s'/M'^2} \rho_i^{\text{OPE}}(s, s', q^2). \quad (26)$$

We provide a detailed examples of the elements of $\rho_i(s, s', q^2)$ for the $\gamma_\mu \gamma_5$ structure as a case study in the Appendix.

Subsequently, we evaluate the necessary sum rules to achieve the form factors required for numerical calculations by equating the corresponding coefficients from both the physical and QCD sides for the different Lorentz structures. This study outlines the sum rules related to form factors, expressing them through baryon masses and their residues. Additionally, it incorporates QCD parameters, including quark and gluon condensates, as well as the masses of quarks. The analysis also involves auxiliary parameters such as M^2 , M'^2 , s_0 , s'_0 , and β .

III. NUMERICAL ANALYSIS

The form factors provide all the essential information needed to specify the decay width of the semileptonic decay. The primary goal in this section is to explore the q^2 dependence of the form factors across the entire physical range. The masses of the particles involved in our numerical calculations are outlined in Table I. We have show the lifetimes

TABLE I: Some input masses used in our numerical calculations.

Parameters	Values
m_e	0.51 MeV [85]
m_μ	105 MeV [85]
m_τ	(1776.09 \pm 0.007) MeV [85]
m_c	(1.27 \pm 0.02) GeV [85]
m_b	(4.18 \pm 0.007) GeV [85]
$m_{\Xi_{cc}}$	(3.62 \pm 0.0015) GeV [85]
$m_{\Omega_{cc}}$	(3.70 \pm 0.09) GeV [9]
$m_{\Xi_{bb}}$	(9.97 \pm 0.19) GeV [9]
$m_{\Omega_{bb}}$	(9.98 \pm 0.18) GeV [9]
m_{Ξ_c}	(2.46 \pm 0.00023) GeV [85]
$m_{\Xi'_c}$	(2.46 \pm 0.00023) GeV [85]
m_{Ω_c}	(2.69 \pm 0.0017) GeV [85]
m_{Λ_c}	(2.28 \pm 0.00014) GeV [85]
m_{Σ_c}	(2.45 \pm 0.00014) GeV [85]
m_{Ξ_b}	(5.79 \pm 0.0006) GeV [85]
$m_{\Xi'_b}$	(5.93 \pm 0.0005) GeV [85]
m_{Λ_b}	(5.61 \pm 0.00017) GeV [85]
m_{Σ_b}	(5.81 \pm 0.00025) GeV [85]

of the doubly heavy baryons in Table II.

TABLE II: Lifetimes (in units of fs) of doubly heavy baryons.

baryons	Ξ_{cc}^{++}	Ξ_{cc}^+	Ω_{cc}^+	Ξ_{bb}^0	Ξ_{bb}^-	Ω_{bb}^-
lifetimes	256 [85]	33 [85]	270 [91]	370 [92]	370 [92]	800 [91]

Also, in Tables III, IV and V, the residue values are included for doubly heavy baryons and single charm and bottom baryons, respectively.

For the condensate parameters, we utilize some inputs parameters as [88–90]: $\langle \bar{q}q \rangle = -(0.24 \pm 0.01) \text{GeV}^3$, $\langle \bar{s}s \rangle = (0.8 \pm 0.2) \langle \bar{q}q \rangle$, $\langle \bar{q}g_s \sigma G q \rangle = m_0^2 \langle \bar{q}q \rangle$, $\langle \bar{s}g_s \sigma G s \rangle = m_0^2 \langle \bar{s}s \rangle$, $m_0^2 = (0.8 \pm 0.2) \text{ GeV}^2$, $\langle \frac{\alpha_s G}{\pi} \rangle = (0.012 \pm 0.004) \text{ GeV}^4$ and for Fermi constant and CKM matrix elements we use [85]:

$$G_F = 1.166 \times 10^{-5} \text{ GeV}^{-2},$$

TABLE III: Residues (in units of GeV^3) of doubly heavy baryons.

Baryons	Ξ_{cc}	Ω_{cc}	Ξ_{bb}	Ω_{bb}
Residues	0.16 ± 0.04 [9]	0.17 ± 0.04 [9]	0.45 ± 0.08 [9]	0.46 ± 0.08 [9]

TABLE IV: Residues (in units of GeV^3) of single charm baryons.

Baryons	Ξ_c	Ξ'_c	Ω_c	Λ_c	Σ_c
Residues	0.027 ± 0.004 [86]	0.055 ± 0.007 [87]	0.093 ± 0.023 [87]	0.022 ± 0.008 [86]	0.045 ± 0.015 [87]

TABLE V: Residues (in units of GeV^3) of single bottom baryons.

Baryons	Ξ_b	Ξ'_b	Λ_b	Σ_b
Residues	0.032 ± 0.009 [86]	0.079 ± 0.020 [87]	0.030 ± 0.009 [86]	0.062 ± 0.018 [87]

$$\begin{aligned} |V_{ub}| &= 0.00357, \\ |V_{cd}| &= 0.225, \quad |V_{cs}| = 0.974. \end{aligned} \tag{27}$$

The sum rules for the form factors involve five additional auxiliary parameters: the Borel parameters M^2 and M'^2 , the continuum thresholds s_0 and s'_0 , and the mixing parameter β . Ideally, these physical quantities should show minimal sensitivity to these parameters. For this aim, we identify particular intervals for these parameters to guarantee that the form factors display minimal sensitivity to their variations. These intervals are defined according to fundamental criteria, including a minimal dependence on any auxiliary parameter, pole dominance, and the convergence of the OPE.

The maximum values for the Borel mass parameters M^2 and M'^2 are established to certify that the pole contributions exceed those from higher states and the continuum. Therefore, we require

$$PC = \frac{\Pi^{OPE}(M^2, M'^2, s_0, s'_0)}{\Pi^{OPE}(M^2, M'^2, \infty, \infty)} \geq 0.5. \tag{28}$$

We determine the minimum values for the Borel mass parameters M^2 and M'^2 by analyzing the necessary conditions for the convergence of the OPE. For effective convergence, it is crucial that the contributions from perturbative processes surpass those from nonperturbative effects. Additionally, we must guarantee that the influence of nonperturbative operators decreases with increasing dimensions. To achieve this, we introduce ratio (R) and employ the following condition:

$$R(M^2, M'^2) = \frac{\Pi^{OPE-dim5}(M^2, M'^2, s_0, s'_0)}{\Pi^{OPE}(M^2, M'^2, s_0, s'_0)} \leq 0.05. \tag{29}$$

According to these specifications, the effective ranges for the Borel mass parameters are outlined in Table VI. The continuum thresholds s_0 and s'_0 are not chosen arbitrarily and we carefully choose these parameters to eliminate any influence from excited states in our calculations. This involves determining specific thresholds by evaluating the stability of sum rules over particular ranges of the Borel mass parameters M^2 and M'^2 . To ensure both stability and physical accuracy, we define s_0 and s'_0 to represent the beginning of the continuum in the spectrum, thereby minimizing contributions from higher states and continuum. This selection process leads us to roughly working regions for the continuum thresholds, which are defined in Table VI as well.

As illustrated in Figs. 4 and 5 (note that we present all the figures for only the transition $\Omega_{bb}^- \rightarrow \Xi_b^0 \ell \bar{\nu}_\ell$, as an example, in the present section), the form factors show remarkable stability across variations in the parameters M^2 , M'^2 , s_0 , and s'_0 within their individual ranges. This consistency indicates that the parameters have been successfully refined, guaranteeing acceptable outcomes across the specified intervals.

The parameters M^2 , M'^2 , s_0 , and s'_0 hold significance, but the parameter β is also essential. Unlike the others, β has no defined boundaries, allowing it to range from $-\infty$ to ∞ . To determine the most suitable range for β , we introduce the transformation $x = \cos \theta$, where $\theta = \tan^{-1} \beta$. We choose the range for x to ensure stability in the form factors, avoiding substantial alterations. For instance, as shown in Fig. 6, the behavior of the F1 form factor in relation to $\cos \theta$ (or x) is illustrated. Consequently, we limit x to the regions $-1 \leq x \leq -0.5$ and $0.5 \leq x \leq 1$. This restriction applies across all six form factors. Figure 6 highlights that the F1 form factor remains relatively stable, especially near the Ioffe current at $x = -0.71$ within the selected negative interval.

Channel	Borel mass (GeV ²)	Continuum threshold (GeV ²)
Λ_c	[3 – 5]	[6.60 – 7.60]
Ξ_c, Σ_c	[3 – 5]	[7.60 – 8.70]
Ξ'_c	[3 – 5]	[8.20 – 9.40]
Ω_c	[3 – 5]	[9.00 – 10.20]
Λ_b	[5.5 – 6.5]	[32.60 – 36.60]
Ξ_b, Σ_b	[5.5 – 6.5]	[35.00 – 39.00]
Ξ'_b	[5.5 – 6.5]	[36.60 – 40.60]
Ξ_{cc}, Ω_{cc}	[4 – 6]	[15.00 – 18.00]
Ξ_{bb}, Ω_{bb}	[10 – 15]	[112.00 – 118.00]

TABLE VI: Working regions of the Borel mass parameters, M^2 or M'^2 , and the continuum thresholds, s_0 or s'_0 , for various channels.

Once we have established the operational ranges for the auxiliary parameters, we move on to explore how the form factors vary with respect to q^2 . By examining the form factors in relation to q^2 , we find that they are well-fit to the subsequent function:

$$\mathcal{F}(q^2) = \frac{\mathcal{F}(0)}{\left(1 - a_1 \frac{q^2}{m_B^2} + a_2 \frac{q^4}{m_B^4} + a_3 \frac{q^6}{m_B^6} + a_4 \frac{q^8}{m_B^8}\right)}. \quad (30)$$

Tables VII to XX present the parameters $\mathcal{F}(0)$, a_1 , a_2 , a_3 , and a_4 derived from the central values of the auxiliary parameters for all decay channels. These parameters correspond to six form factors: F_1 , F_2 , F_3 , G_1 , G_2 , and G_3 , which are related to the structures $p'\gamma_\mu$, $p_\mu p''\not{p}$, $p'_\mu p''\not{p}$, $\gamma_\mu\gamma_5$, $p_\mu p''\not{p}\gamma_5$ and $p'_\mu\gamma_5$, respectively.

TABLE VII: The fit function parameters of different form factors for $\Xi_{cc}^{++} \rightarrow \Lambda_c^+ \bar{\ell} \nu_\ell$ transition.

Parameter	$F_1(q^2)$	$F_2(q^2)$	$F_3(q^2)$	$G_1(q^2)$	$G_2(q^2)$	$G_3(q^2)$
$\mathcal{F}(q^2 = 0)$	-0.31 ± 0.11	1.24 ± 0.40	0.10 ± 0.03	0.16 ± 0.04	1.23 ± 0.33	-1.55 ± 0.55
a_1	2.63	-0.05	2.99	2.97	2.06	2.18
a_2	4.63	-111.38	18.17	35.71	-4.36	-22.28
a_3	36.98	1329.88	-440.35	-432.60	-448.83	321.21
a_4	-658.06	-5206.92	2300.78	1401.78	2947.41	-1972.39

TABLE VIII: The fit function parameters of different form factors for $\Xi_{cc}^+ \rightarrow \Xi_c^0 \bar{\ell} \nu_\ell$ transition.

Parameter	$F_1(q^2)$	$F_2(q^2)$	$F_3(q^2)$	$G_1(q^2)$	$G_2(q^2)$	$G_3(q^2)$
$\mathcal{F}(q^2 = 0)$	-0.37 ± 0.13	1.35 ± 0.43	0.14 ± 0.06	0.20 ± 0.06	1.34 ± 0.43	-1.82 ± 0.65
a_1	1.54	-0.05	1.99	2.79	1.07	2.15
a_2	-23.84	-111.38	17.17	35.82	-78.83	-27.91
a_3	268.50	1329.88	-442.35	-541.92	935.73	449.20
a_4	-1174.79	-5206.92	2372.78	2240.25	-3550.64	-2702.99

TABLE IX: The fit function parameters of different form factors for $\Omega_{cc}^+ \rightarrow \Xi_c^0 \bar{\ell} \nu_\ell$ transition.

Parameter	$F_1(q^2)$	$F_2(q^2)$	$F_3(q^2)$	$G_1(q^2)$	$G_2(q^2)$	$G_3(q^2)$
$\mathcal{F}(q^2 = 0)$	-0.33 ± 0.12	1.41 ± 0.50	0.12 ± 0.04	0.17 ± 0.04	1.41 ± 0.33	-1.66 ± 0.55
a_1	2.79	0.15	10.14	3.16	-0.91	2.31
a_2	5.22	-119.98	71.54	40.25	-84.24	-25.11
a_3	36.98	1329.88	-440.35	-432.60	-448.83	384.40
a_4	-836.33	-5290.92	1886.22	1781.08	-2879.86	-2506.09

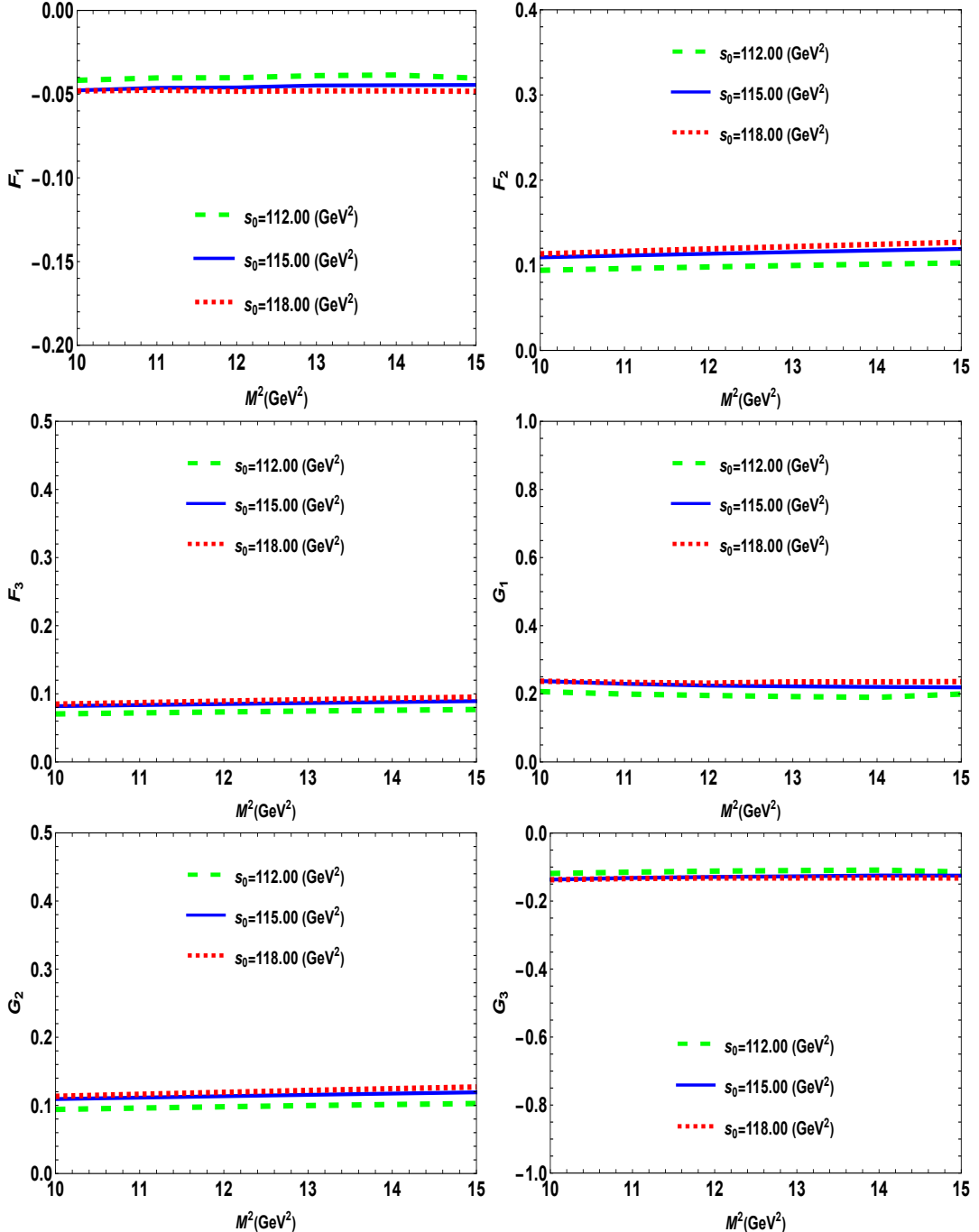


FIG. 4: Form factors of $\Omega_{bb}^- \rightarrow \Xi_b^0 \ell \bar{\nu}_\ell$, as an example, as a function of the Borel parameter M^2 for various s_0 amounts, with $q^2 = 0$ and other auxiliary parameters set to their central values. The graphs represent the structures $\not{p}' \gamma_\mu$, $p_\mu \not{p}' \not{p}$, $p'_\mu \not{p}' \not{p}$, $\gamma_\mu \gamma_5$, $p_\mu \not{p}' \gamma_5$, and $p'_\mu \gamma_5$ corresponding to F_1 , F_2 , F_3 , G_1 , G_2 , and G_3 , respectively.

QCD sum rule approach proposes various structures for the choosing form factors. By examining the Borel and continuum ranges alongside the x parameter, we can make effective selections that minimize uncertainties in the outcomes. As mentioned, the six structures chosen— $\not{p}' \gamma_\mu$, $p_\mu \not{p}' \not{p}$, $p'_\mu \not{p}' \not{p}$, $\gamma_\mu \gamma_5$, $p_\mu \not{p}' \gamma_5$ and $p'_\mu \gamma_5$ —are aligned with the desired form factors F_1 , F_2 , F_3 , G_1 , G_2 and G_3 , respectively.

The uncertainties associated with the form factors stem from the variability in auxiliary parameter ranges and uncertainties in other input values. In Figures 7 and 8, we depict the form factors F_1 , F_2 , F_3 , G_1 , G_2 , and G_3 as functions of q^2 at the central values of s_0 , s'_0 , M^2 , M'^2 , and at the Ioffe point $x = -0.71$ without and with

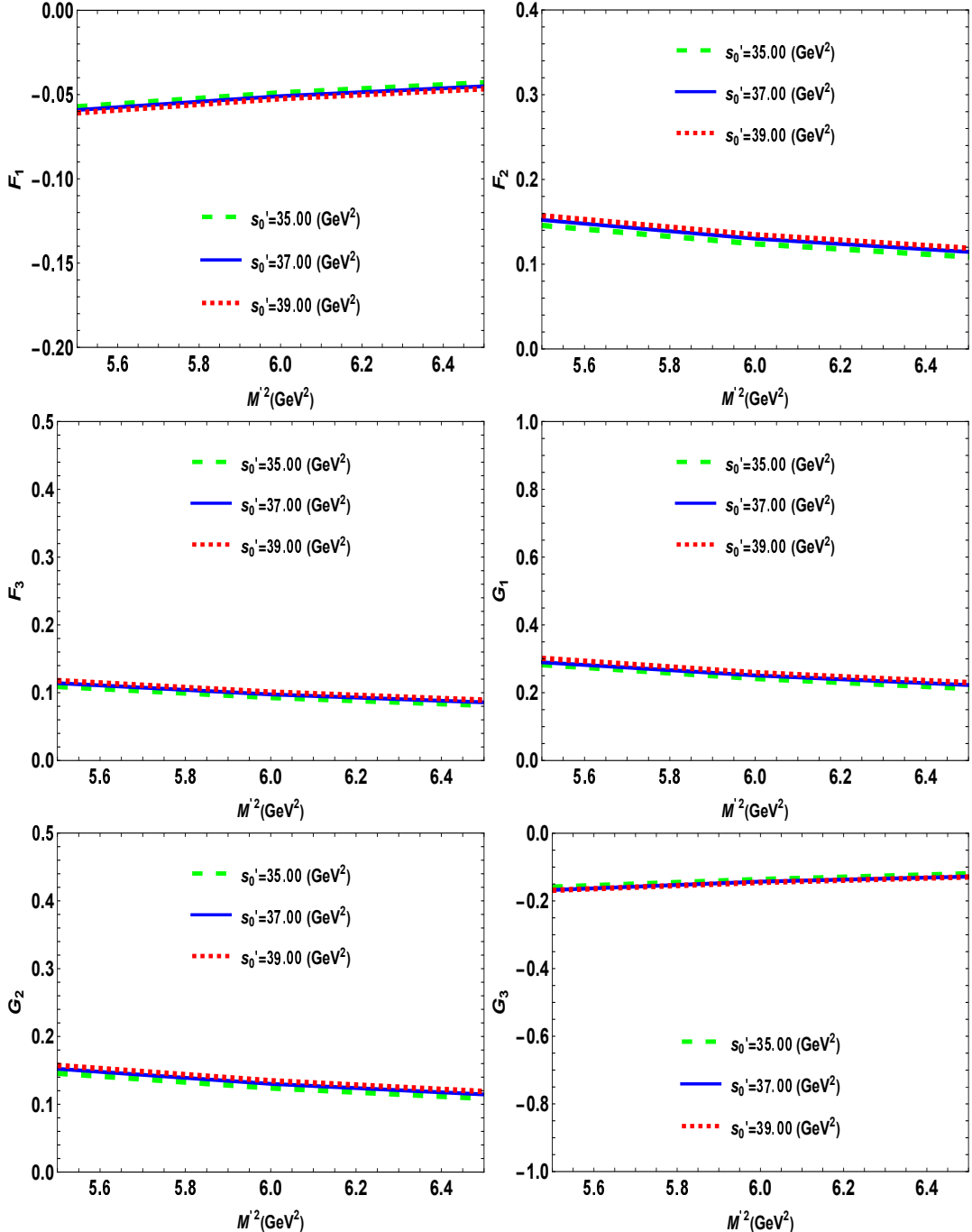


FIG. 5: Form factors of $\Omega_{bb}^- \rightarrow \Xi_b^0 \ell \bar{\nu}_\ell$, as an example, as a function of the Borel parameter M'^2 for various s'_0 amounts, with $q^2 = 0$ and other auxiliary parameters set to their central values. The graphs represent the structures $\not{p}' \gamma_\mu$, $p_\mu \not{p}' \not{p}$, $p'_\mu \not{p}' \not{p}$, $\gamma_\mu \gamma_5$, $p_\mu \not{p}' \gamma_5$, and $p'_\mu \gamma_5$ corresponding to F_1 , F_2 , F_3 , G_1 , G_2 , and G_3 , respectively.

uncertainties, respectively.

As expected for weak transitions, there is a trend of increasing form factors with higher q^2 . In the next section, we will apply the fitted expressions for these six form factors within the range $m_t^2 \leq q^2 \leq (m_B - m_{B'})^2$ to evaluate the decay widths and branching ratios.

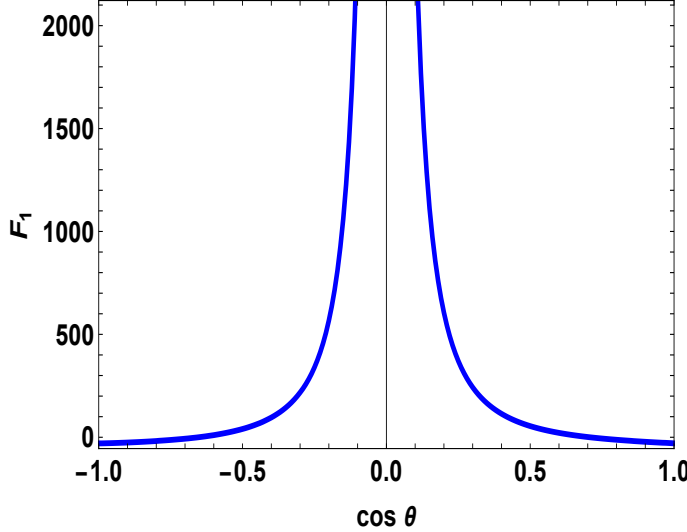


FIG. 6: The form factor F_1 of $\Omega_{bb}^- \rightarrow \Xi_b^0 \ell \bar{\nu}_\ell$ transition, as an example, as a function of $\cos \theta$ (or x) at $q^2 = 0$ and average amounts of other auxiliary parameters, related to the $\not{p}' \gamma_\mu$ structure.

TABLE X: The fit function parameters of different form factors for $\Xi_{cc}^{++} \rightarrow \Sigma_c^+ \bar{\ell} \nu_\ell$ transition.

Parameter	$F_1(q^2)$	$F_2(q^2)$	$F_3(q^2)$	$G_1(q^2)$	$G_2(q^2)$	$G_3(q^2)$
$\mathcal{F}(q^2 = 0)$	-1.55 ± 0.50	0.44 ± 0.13	0.54 ± 0.21	-1.02 ± 0.37	0.44 ± 0.13	-1.19 ± 0.39
a_1	2.34	2.81	4.46	1.91	2.37	2.48
a_2	-21.47	-50.88	-36.46	-24.95	-69.49	-35.56
a_3	326.25	756.81	540.92	424.87	972.75	551.08
a_4	-1892.28	-3130.44	-1827.97	-1989.49	-3861.41	-3598.57

TABLE XI: The fit function parameters of different form factors for $\Xi_{cc}^{++} \rightarrow \Xi_c' \bar{\ell} \nu_\ell$ transition.

Parameter	$F_1(q^2)$	$F_2(q^2)$	$F_3(q^2)$	$G_1(q^2)$	$G_2(q^2)$	$G_3(q^2)$
$\mathcal{F}(q^2 = 0)$	-1.67 ± 0.60	0.47 ± 0.17	0.67 ± 0.27	-1.11 ± 0.39	0.47 ± 0.15	-1.28 ± 0.44
a_1	2.83	2.81	5.14	2.32	4.69	2.98
a_2	3.49	-48.68	1.87	-2.23	35.33	-15.14
a_3	-98.02	940.09	124.19	34.22	-953.32	266.54
a_4	488.55	-5210.79	-603.14	320.73	7132.38	-2302.21

TABLE XII: The fit function parameters of different form factors for $\Xi_{cc}^+ \rightarrow \Sigma_c^0 \bar{\ell} \nu_\ell$ transition.

Parameter	$F_1(q^2)$	$F_2(q^2)$	$F_3(q^2)$	$G_1(q^2)$	$G_2(q^2)$	$G_3(q^2)$
$\mathcal{F}(q^2 = 0)$	-1.55 ± 0.50	0.44 ± 0.13	0.54 ± 0.21	-1.02 ± 0.37	0.44 ± 0.13	-1.19 ± 0.39
a_1	2.34	2.81	4.46	1.91	2.37	2.48
a_2	-21.47	-50.88	-36.46	-24.95	-69.49	-35.56
a_3	326.25	756.81	540.92	424.87	972.75	551.08
a_4	-1892.28	-3130.44	-1827.97	-1989.49	-3861.41	-3598.57

IV. CALCULATION OF DECAY WIDTHS AND BRANCHING RATIOS

In this section, we define our calculations for key physical observables, including the decay widths and branching ratios related to the semileptonic transitions focusing on all possible lepton channels. To do this, we will apply the derived fit functions for the form factors discussed earlier. By using the effective Hamiltonian presented in Eq. (1), we will analyze the decay widths and branching ratios. This process incorporates helicity amplitudes for both vector

TABLE XIII: The fit function parameters of different form factors for $\Xi_{cc}^+ \rightarrow \Xi_c'^0 \bar{\ell} \nu_\ell$ transition.

Parameter	$F_1(q^2)$	$F_2(q^2)$	$F_3(q^2)$	$G_1(q^2)$	$G_2(q^2)$	$G_3(q^2)$
$\mathcal{F}(q^2 = 0)$	-1.67 ± 0.60	0.47 ± 0.17	0.67 ± 0.27	-1.11 ± 0.39	0.47 ± 0.15	-1.28 ± 0.44
a_1	2.83	2.81	5.14	2.32	4.69	2.98
a_2	3.49	-48.68	1.87	-2.23	35.33	-15.14
a_3	-98.02	940.09	124.19	34.22	-953.32	266.54
a_4	488.55	-5210.79	-603.14	320.73	7132.38	-2302.21

TABLE XIV: The fit function parameters of different form factors for $\Omega_{cc}^+ \rightarrow \Xi_c'^0 \bar{\ell} \nu_\ell$ transition.

Parameter	$F_1(q^2)$	$F_2(q^2)$	$F_3(q^2)$	$G_1(q^2)$	$G_2(q^2)$	$G_3(q^2)$
$\mathcal{F}(q^2 = 0)$	-1.41 ± 0.49	0.46 ± 0.13	0.54 ± 0.21	-0.90 ± 0.34	0.46 ± 0.11	-1.08 ± 0.32
a_1	2.94	1.09	4.44	3.45	0.77	2.88
a_2	-10.29	-69.88	-11.46	-42.55	-89.86	-28.33
a_3	200.95	748.81	313.38	-858.65	1154.75	478.46
a_4	-1542.68	-2826.30	-740.11	4714.66	-5448.96	-3660.69

TABLE XV: The fit function parameters of different form factors for $\Omega_{cc}^+ \rightarrow \Omega_c^0 \bar{\ell} \nu_\ell$ transition.

Parameter	$F_1(q^2)$	$F_2(q^2)$	$F_3(q^2)$	$G_1(q^2)$	$G_2(q^2)$	$G_3(q^2)$
$\mathcal{F}(q^2 = 0)$	-1.00 ± 0.30	0.33 ± 0.12	0.42 ± 0.17	-0.64 ± 0.27	0.33 ± 0.11	-0.76 ± 0.34
a_1	2.94	4.52	2.52	3.48	87.48	2.88
a_2	-10.29	-9.11	-85.48	36.29	-77.20	-28.33
a_3	200.99	-29.44	134.26	-647.83	749.89	478.46
a_4	-1542.55	1408.79	5181.55	4371.73	-1849.93	-3660.69

TABLE XVI: The fit function parameters of different form factors for $\Xi_{bb}^- \rightarrow \Lambda_b^0 \ell \bar{\nu}_\ell$ transition.

Parameter	$F_1(q^2)$	$F_2(q^2)$	$F_3(q^2)$	$G_1(q^2)$	$G_2(q^2)$	$G_3(q^2)$
$\mathcal{F}(q^2 = 0)$	-0.04 ± 0.02	0.10 ± 0.04	0.07 ± 0.03	0.23 ± 0.04	0.10 ± 0.05	-0.11 ± 0.04
a_1	3.32	9.18	8.70	3.31	9.18	1.58
a_2	3.68	34.84	20.67	13.82	34.84	-43.91
a_3	-42.06	-35.80	67.08	-172.13	-35.80	374.18
a_4	98.43	-69.53	-292.34	535.16	-69.53	-1103.82

TABLE XVII: The fit function parameters of different form factors for $\Omega_{bb}^- \rightarrow \Xi_b^0 \ell \bar{\nu}_\ell$ transition.

Parameter	$F_1(q^2)$	$F_2(q^2)$	$F_3(q^2)$	$G_1(q^2)$	$G_2(q^2)$	$G_3(q^2)$
$\mathcal{F}(q^2 = 0)$	-0.04 ± 0.01	0.11 ± 0.05	0.08 ± 0.02	0.22 ± 0.08	0.11 ± 0.03	-0.12 ± 0.03
a_1	3.60	8.48	8.00	4.18	8.48	1.21
a_2	8.94	18.09	4.22	35.05	18.09	-53.85
a_3	-77.06	98.05	197.69	-364.71	98.05	462.03
a_4	175.13	-420.77	-632.86	-420.77	-1353.90	-1173.87

TABLE XVIII: The fit function parameters of different form factors for $\Xi_{bb}^0 \rightarrow \Sigma_b^+ \ell \bar{\nu}_\ell$ transition.

Parameter	$F_1(q^2)$	$F_2(q^2)$	$F_3(q^2)$	$G_1(q^2)$	$G_2(q^2)$	$G_3(q^2)$
$\mathcal{F}(q^2 = 0)$	-0.04 ± 0.01	0.21 ± 0.09	0.014 ± 0.005	0.018 ± 0.008	0.25 ± 0.09	-0.37 ± 0.13
a_1	5.47	8.55	7.96	3.98	8.55	3.84
a_2	-1.14	20.34	33.15	0.03	20.34	-7.95
a_3	82.00	79.30	-95.63	-3.64	79.30	105.66
a_4	-225.92	-372.25	170.86	39.17	-372.25	-294.28

TABLE XIX: The fit function parameters of different form factors for $\Xi_b^- \rightarrow \Sigma_b^0 \ell \bar{\nu}_\ell$ transition.

Parameter	$F_1(q^2)$	$F_2(q^2)$	$F_3(q^2)$	$G_1(q^2)$	$G_2(q^2)$	$G_3(q^2)$
$\mathcal{F}(q^2 = 0)$	-0.04 ± 0.01	0.21 ± 0.09	0.014 ± 0.005	0.018 ± 0.008	0.25 ± 0.09	-0.37 ± 0.13
a_1	5.47	8.55	7.96	3.98	8.55	3.84
a_2	-1.14	20.34	33.15	0.03	20.34	-7.95
a_3	82.00	79.30	-95.63	-3.64	79.30	105.66
a_4	-225.92	-372.25	170.86	39.17	-372.25	-294.28

TABLE XX: The fit function parameters of different form factors for $\Omega_b^- \rightarrow \Xi_b' \ell \bar{\nu}_\ell$ transition.

Parameter	$F_1(q^2)$	$F_2(q^2)$	$F_3(q^2)$	$G_1(q^2)$	$G_2(q^2)$	$G_3(q^2)$
$\mathcal{F}(q^2 = 0)$	-0.06 ± 0.02	0.34 ± 0.15	0.02 ± 0.01	0.27 ± 0.09	-0.57 ± 0.23	-0.12 ± 0.03
a_1	5.45	9.98	10.15	3.88	9.98	3.96
a_2	-1.98	55.96	55.55	-3.05	55.96	-4.71
a_3	89.84	-222.90	-145.40	32.45	-222.90	75.46
a_4	-248.79	472.05	81.56	-47.00	472.06	-203.39

and axial vector currents, which we present below:

$$\begin{aligned} H_{\frac{1}{2},0}^V &= -i \frac{\sqrt{Q_-}}{\sqrt{q^2}} \left((M_1 + M_2) F_1 - \frac{q^2}{M_1} F_2 \right), \quad H_{\frac{1}{2},0}^A = -i \frac{\sqrt{Q_+}}{\sqrt{q^2}} \left((M_1 - M_2) G_1 + \frac{q^2}{M_1} G_2 \right), \\ H_{\frac{1}{2},1}^V &= i \sqrt{2Q_-} \left(-F_1 + \frac{M_1 + M_2}{M_1} F_2 \right), \quad H_{\frac{1}{2},1}^A = i \sqrt{2Q_+} \left(-G_1 - \frac{M_1 - M_2}{M_1} G_2 \right), \\ H_{\frac{1}{2},t}^V &= -i \frac{\sqrt{Q_+}}{\sqrt{q^2}} \left((M_1 - M_2) F_1 + \frac{q^2}{M_1} F_3 \right), \quad H_{\frac{1}{2},t}^A = -i \frac{\sqrt{Q_-}}{\sqrt{q^2}} \left((M_1 + M_2) G_1 - \frac{q^2}{M_1} G_3 \right), \end{aligned} \quad (31)$$

where M_1 and M_2 represent the masses of the initial and the final baryon, respectively. The variable Q_\pm is defined as $Q_\pm = (M_1 \pm M_2)^2 - q^2$. These helicity amplitudes play a vital role in calculating the decay widths and branching ratios. The amplitudes corresponding to negative helicity are given by:

$$H_{-\lambda_2, -\lambda_W}^V = H_{\lambda_2, \lambda_W}^V \quad \text{and} \quad H_{-\lambda_2, -\lambda_W}^A = -H_{\lambda_2, \lambda_W}^A, \quad (32)$$

where λ_2 and λ_W represent the polarizations of the final baryon and the W boson, respectively. Lastly, the helicity amplitudes for the $V - A$ current are detailed as follows:

$$H_{\lambda_2, \lambda_W} = H_{\lambda_2, \lambda_W}^V - H_{\lambda_2, \lambda_W}^A. \quad (33)$$

The decay width, considering both longitudinally and transversely polarized $\ell \bar{\nu}_\ell$ pairs, is calculated as follows:

$$\frac{d\Gamma_L}{dq^2} = \frac{G_F^2 |V_{CKM}|^2 q^2 |\mathbf{p}'| (1 - \hat{m}_l^2)^2}{384\pi^3 M_1^2} \left((2 + \hat{m}_l^2)(|H_{-\frac{1}{2},0}|^2 + |H_{\frac{1}{2},0}|^2) + 3\hat{m}_l^2(|H_{-\frac{1}{2},t}|^2 + |H_{\frac{1}{2},t}|^2) \right), \quad (34)$$

$$\frac{d\Gamma_T}{dq^2} = \frac{G_F^2 |V_{CKM}|^2 q^2 |\mathbf{p}'| (1 - \hat{m}_l^2)^2 (2 + \hat{m}_l^2)}{384\pi^3 M_1^2} (|H_{\frac{1}{2},1}|^2 + |H_{-\frac{1}{2},-1}|^2), \quad (35)$$

where $\hat{m}_l \equiv m_l/\sqrt{q^2}$, and $\mathbf{p}' = \sqrt{Q_+ Q_-}/(2M_1)$ is the magnitude of three momentum of final baryon in the rest frame of initial baryon. After integrating over the q^2 , we gain the total decay width as follow:

$$\Gamma = \int_{m_l^2}^{(M_1 - M_2)^2} dq^2 \frac{d\Gamma}{dq^2}, \quad (36)$$

where

$$\frac{d\Gamma}{dq^2} = \frac{d\Gamma_L}{dq^2} + \frac{d\Gamma_T}{dq^2}. \quad (37)$$

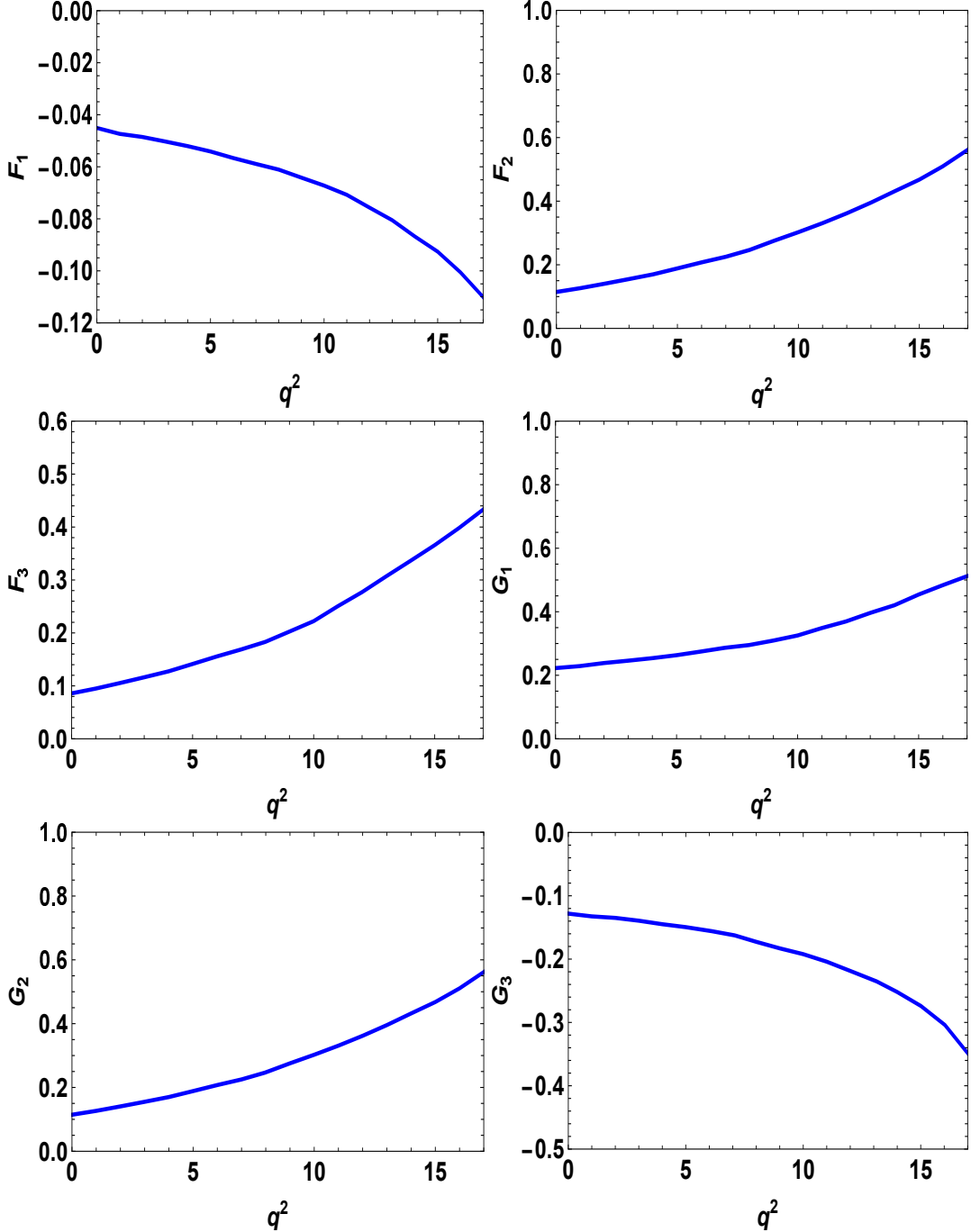


FIG. 7: Form factors of $\Omega_{bb}^- \rightarrow \Xi_b^0 \ell \bar{\nu}_\ell$, as an example, as functions of q^2 at the central values of auxiliary parameters and the Ioffe point for the chosen structures.

After analyzing the decay width for all decay channels, we present the average values and their uncertainties in Tables [XXI](#), [XXII](#), [XXIII](#), [XXIV](#) and [XXV](#).

Additionally, we evaluate the branching ratios for all decay channels, and present the obtained results in Tables [XXI](#), [XXII](#), [XXIII](#), [XXIV](#) and [XXV](#). It's worth noting that our results exhibit relatively small uncertainties, indicating a successful optimization regarding variations in auxiliary parameters. These findings clear the way for verification through future experimental efforts.

TABLE XXI: Decay widths and branching ratios results of cc sector for the e^+ channels. It should be noted that the results of the $\Xi_{cc}^{++} \rightarrow \Xi_c^+ \bar{\ell} \nu_\ell$ decay channel come from our previous work [46] for the table consistency.

Channel	$\Gamma/(10^{-14} \text{ GeV})$	$\mathcal{B}/10^{-3}$
$\Xi_{cc}^{++} \rightarrow \Lambda_c^+ e^+ \nu_e$	$1.07^{+0.10}_{-0.12}$	4.19 ± 0.82
$\Xi_{cc}^{++} \rightarrow \Xi_c^+ e^+ \nu_e$	$7.20^{+0.77}_{-0.59}$	$2.80^{+0.49}_{-0.13}$
$\Xi_{cc}^+ \rightarrow \Xi_c^0 e^+ \nu_e$	$7.20^{+0.77}_{-0.59}$	$4.81^{+0.49}_{-0.43}$
$\Omega_{cc}^+ \rightarrow \Xi_c^0 e^+ \nu_e$	$0.72^{+0.11}_{-0.13}$	2.28 ± 0.48
$\Xi_{cc}^{++} \rightarrow \Sigma_c^+ e^+ \nu_e$	5.05 ± 0.77	19.65 ± 1.39
$\Xi_{cc}^{++} \rightarrow \Xi_c' e^+ \nu_e$	$63.77^{+4.20}_{-4.22}$	$248.10^{+11.30}_{-10.23}$
$\Xi_{cc}^+ \rightarrow \Sigma_c^0 e^+ \nu_e$	4.19 ± 0.51	3.37 ± 0.31
$\Xi_{cc}^+ \rightarrow \Xi_c' e^+ \nu_e$	$63.77^{+4.20}_{-4.22}$	$42.64^{+1.30}_{-1.33}$
$\Omega_{cc}^+ \rightarrow \Xi_c' e^+ \nu_e$	4.19 ± 0.42	13.13 ± 0.86
$\Omega_{cc}^+ \rightarrow \Omega_c^0 e^+ \nu_e$	$21.86^{+1.10}_{-1.09}$	$68.46^{+4.30}_{-4.23}$

TABLE XXII: Decay widths and branching ratios results of cc sector for the μ^+ channels. It should be noted that the results of the $\Xi_{cc}^{++} \rightarrow \Xi_c^+ \bar{\ell} \nu_\ell$ decay channel come from our previous work [46] for the table consistency.

Channel	$\Gamma/(10^{-14} \text{ GeV})$	$\mathcal{B}/10^{-3}$
$\Xi_{cc}^{++} \rightarrow \Lambda_c^+ \mu^+ \nu_\mu$	1.06 ± 0.11	4.13 ± 0.83
$\Xi_{cc}^{++} \rightarrow \Xi_c^+ \mu^+ \nu_\mu$	$7.01^{+0.66}_{-0.35}$	$2.72^{+0.47}_{-0.13}$
$\Xi_{cc}^+ \rightarrow \Xi_c^0 \mu^+ \nu_\mu$	$7.01^{+0.66}_{-0.35}$	$4.68^{+0.19}_{-0.13}$
$\Omega_{cc}^+ \rightarrow \Xi_c^0 \mu^+ \nu_\mu$	$0.71^{+0.11}_{-0.12}$	2.23 ± 0.44
$\Xi_{cc}^{++} \rightarrow \Sigma_c^+ \mu^+ \nu_\mu$	4.91 ± 0.72	19.10 ± 1.13
$\Xi_{cc}^{++} \rightarrow \Xi_c' \mu^+ \nu_\mu$	$61.48^{+4.21}_{-4.24}$	$239.20^{+10.30}_{-11.23}$
$\Xi_{cc}^+ \rightarrow \Sigma_c^0 \mu^+ \nu_\mu$	4.07 ± 0.50	3.28 ± 0.23
$\Xi_{cc}^+ \rightarrow \Xi_c' \mu^+ \nu_\mu$	$61.48^{+4.21}_{-4.20}$	$41.11^{+1.30}_{-1.23}$
$\Omega_{cc}^+ \rightarrow \Xi_c' \mu^+ \nu_\mu$	4.07 ± 0.40	12.79 ± 0.80
$\Omega_{cc}^+ \rightarrow \Omega_c^0 \mu^+ \nu_\mu$	$21.07^{+1.10}_{-1.08}$	$65.97^{+4.28}_{-4.22}$

TABLE XXIII: Decay widths and branching ratios results of bb sector for the e channels.

Channel	$\Gamma/(10^{-16} \text{ GeV})$	$\mathcal{B}/10^{-4}$
$\Xi_{bb}^- \rightarrow \Lambda_b^0 e \bar{\nu}_e$	2.01 ± 0.23	$1.13^{+0.16}_{-0.18}$
$\Omega_{bb}^- \rightarrow \Xi_b^0 e \bar{\nu}_e$	1.41 ± 0.13	$1.71^{+0.20}_{-0.21}$
$\Xi_{bb}^0 \rightarrow \Sigma_b^+ e \bar{\nu}_e$	$1.61^{+0.16}_{-0.17}$	0.90 ± 0.08
$\Xi_{bb}^- \rightarrow \Sigma_b^0 e \bar{\nu}_e$	$1.61^{+0.16}_{-0.17}$	0.90 ± 0.08
$\Omega_{bb}^- \rightarrow \Xi_b^0 e \bar{\nu}_e$	$1.83^{+0.16}_{-0.18}$	2.22 ± 0.22

TABLE XXIV: Decay widths and branching ratios results of bb sector for the μ channels.

Channel	$\Gamma/(10^{-16} \text{ GeV})$	$\mathcal{B}/10^{-4}$
$\Xi_{bb}^- \rightarrow \Lambda_b^0 \mu \bar{\nu}_\mu$	$2.00^{+0.23}_{-0.21}$	1.12 ± 0.15
$\Omega_{bb}^- \rightarrow \Xi_b^0 \mu \bar{\nu}_\mu$	$1.40^{+0.12}_{-0.13}$	$1.71^{+0.20}_{-0.21}$
$\Xi_{bb}^0 \rightarrow \Sigma_b^+ \mu \bar{\nu}_\mu$	$1.60^{+0.16}_{-0.15}$	0.90 ± 0.08
$\Xi_{bb}^- \rightarrow \Sigma_b^0 \mu \bar{\nu}_\mu$	$1.60^{+0.16}_{-0.15}$	0.90 ± 0.08
$\Omega_{bb}^- \rightarrow \Xi_b^0 \mu \bar{\nu}_\mu$	1.82 ± 0.17	$2.22^{+0.20}_{-0.22}$

TABLE XXV: Decay widths and branching ratios results of bb sector for the τ channels.

Channel	$\Gamma/(10^{-16} \text{ GeV})$	$\mathcal{B}/10^{-4}$
$\Xi_{bb}^- \rightarrow \Lambda_b^0 \tau \bar{\nu}_\tau$	1.14 ± 0.17	0.64 ± 0.10
$\Omega_{bb}^- \rightarrow \Xi_b^0 \tau \bar{\nu}_\tau$	0.74 ± 0.08	0.90 ± 0.11
$\Xi_{bb}^0 \rightarrow \Sigma_b^+ \tau \bar{\nu}_\tau$	1.03 ± 0.10	0.58 ± 0.04
$\Xi_{bb}^- \rightarrow \Sigma_b^0 \tau \bar{\nu}_\tau$	1.03 ± 0.10	0.58 ± 0.04
$\Omega_{bb}^- \rightarrow \Xi_b^0 \tau \bar{\nu}_\tau$	$1.11^{+0.10}_{-0.13}$	$1.35^{+0.15}_{-0.17}$

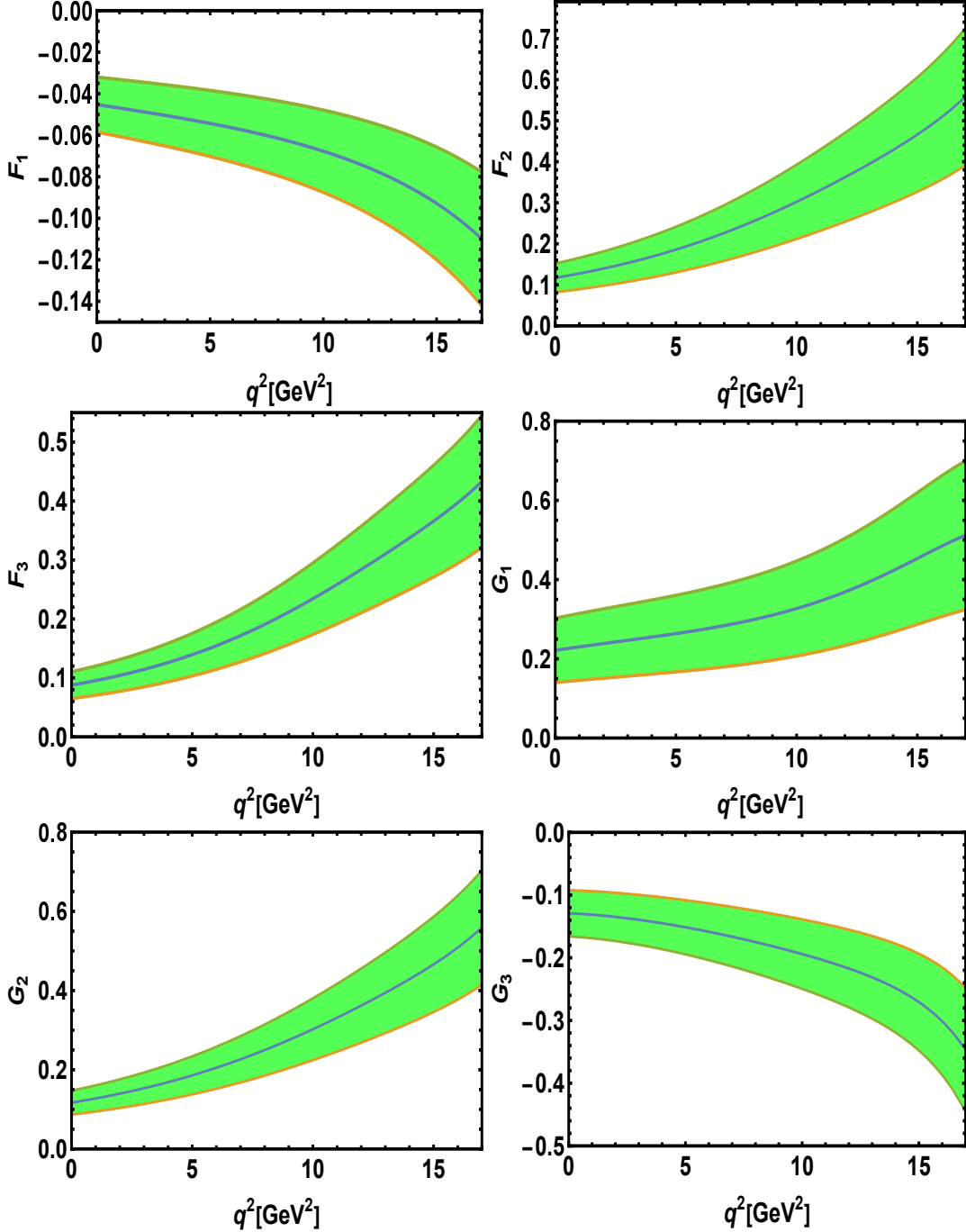


FIG. 8: Form factors and their uncertainties of $\Omega_{bb}^- \rightarrow \Xi_b^0 \ell \bar{\nu}_\ell$, as an example, as functions of q^2 at the central values of auxiliary parameters and the Ioffe point for the chosen structures.

V. CONCLUSION

In conclusion, we investigated the semileptonic decays of the doubly charmed (bottom) baryons into the single heavy baryons using the QCD sum rule approach in all possible lepton channels. We considered the interpolating currents of the involved initial and final baryons with their most possible general forms. Our calculations accounted for nonperturbative operators with mass dimensions up to five, yielding transition form factors characterized through the vector and axial vector transition currents. Following the determination of working intervals of the auxiliary

parameters, we derived the fit functions for six relevant form factors with respect to q^2 within the allowed physical ranges at all considered decay channels. These findings enabled us to estimate decay widths and branching ratios for all possible lepton channels. It should be noted that in the computations we utilized the newly obtained residue and mass values for doubly heavy baryons [9]. We estimated the decay rates and branching fractions for each lepton channel separately, achieving results with minimized uncertainties through careful auxiliary parameter selection.

The identification of the doubly charmed baryon Ξ_{cc} has spurred extensive theoretical investigations into hadron spectroscopy and the decay mechanisms associated with baryons containing two heavy quarks. As experiments like LHCb continue to search for these particles, our analysis emphasizes the need for a deeper understanding of their properties. Despite the intensive theoretical expectations about the doubly heavy baryons, only Ξ_{cc}^{++} has been experimentally confirmed to date. Given advancements from experiments such as LHCb at CERN, we anticipate the soon-to-come discovery of other members of the baryons containing two heavy quarks. Our findings will support experimental teams in this pursuit. The orders of magnitude obtained for branching fractions for the examined weak decays indicate that these semileptonic processes can be achieved and investigated in experiments such as LHCb in near future. Future experimental results related to these observables, compared with our theoretical predictions, will provide crucial information about the internal composition and structure of doubly heavy baryons. This will also allow for accurate evaluations of essential characteristics of these interesting baryons like their mass and lifetime.

ACKNOWLEDGMENTS

K. Azizi thanks Iran national science foundation (INSF) for the partial financial support supplied under the elites Grant No. 4037888. He is also thankful to the CERN-Theory department for their support and hospitality.

APPENDIX: PERTURBATIVE AND NONPERTURBATIVE CONTRIBUTIONS

The explicit expressions for the perturbative and nonperturbative components of the spectral density for the semileptonic transition $\Omega_b^- \rightarrow \Xi_b^0 \ell \bar{\nu}_\ell$, as an example, for the structure $\gamma_\mu \gamma_5$ are shown as:

$$\begin{aligned} \rho_{\gamma_\mu \gamma_5}^{Pert.}(s, s', q^2) = & \int_0^1 du \int_0^{1-u} dv \int_0^{1-u-v} dz \frac{\sqrt{3}}{256 A H^3 J^6 \pi^4} \\ & \left\{ -D_1^2 J^4 \left[B(11 + 7\beta)H(H - 2u)v + z \left(-((11 + 7\beta)CH(1 + 2u)) - 2uz(18u + 7(-1 + \beta)z) + H(v(-40 - 18u \right. \right. \right. \\ & \left. \left. \left. + 7\beta(-2 + v) + 29v) + (-22 + 3u + 29v + 7\beta(-2 - 3u + v))z + (11 + 7\beta)z^2) \right) \right] - 2AH^2 v^2 z \left[H J^2 m_b^2 (A \beta s' \right. \\ & \left. \left. \left. + 4(-q^2 + s)u - s'(5H + u + 5z)) + s'z \left\{ -[(-H + u - z)((5 + \beta)Hs' + 2(2 + \beta)s'u + q^2(u - \beta u) + (5 + \beta)s'z) \right. \right. \right. \\ & \left. \left. \left. (BHv + z(CH + 2Hv + Hz + 2uz)) \right] - s \left[BH(3(1 + \beta)H^2 + 2(2 + \beta)Hu - 6(2 + \beta)u^2)v + z \left(H(-3(1 + \beta) \right. \right. \right. \\ & \left. \left. \left. + (7 + 5\beta)u + 4(2 + \beta)u^2 - 6(2 + \beta)u^3 + [15 - 7u(4 + u) + \beta(15 + (-20 + u)u)]v + 3(-7 - 7\beta + 7u + 5\beta u)v^2 \right. \right. \right. \\ & \left. \left. \left. + 9(1 + \beta)v^3) + (6(-1 + \beta)u^3 + (7 + 5\beta)Hu(-2 + 3v) + 3(1 + \beta)H^2(-3 + 4v))z + (9(1 + \beta)H^2 + (7 + 5\beta)Hu \right. \right. \right. \\ & \left. \left. \left. + 4(2 + \beta)u^2)z^2 + 3(1 + \beta)Hz^3) \right] \right\} \right] - 2D_1 H J^2 v \left\{ 2A(-4 + \beta)H J^2 m_b^2 + uz \left[q^2 \left\{ BHv(-9 + 13u + \beta(3 + 13u - 3v) \right. \right. \right. \\ & \left. \left. \left. + 9v) + z(CH(3(-3 + \beta) + 13(1 + \beta)u) + Hv(4(-9 + 3\beta + 11u + 5\beta u) - 9(-3 + \beta)v) + (-6(-3 + \beta) - 8(5 + \beta)u \right. \right. \right. \\ & \left. \left. \left. + 2(13 + 15\beta)u^2 + 15(-3 + \beta)v + 8(5 + \beta)uv - 9(-3 + \beta)v^2)z + (9(H + 2u) + \beta(3 - 2u - 3v))z^2 \right) \right\} + s \left(BHv(5 + \beta \right. \\ & \left. \left. + 2u + 2\beta u - (5 + \beta)v) + z[CH(5 + \beta + 2(1 + \beta)u) + Hv(24 - 4(4 + 3\beta)u + (-19 + \beta)v) + (-10 - 2\beta + 21u \right. \right. \right. \\ & \left. \left. \left. - 3\beta u - 16u^2 - 28\beta u^2 + (29 + \beta + 3(-7 + \beta)u)v + (-19 + \beta)v^2)z + (5 + \beta - 18u + 2\beta u - (5 + \beta)v)z^2] \right) \right] + 2s'z \\ & \left[2BHv(5 + \beta + 5u + \beta u - 11u^2 - 6\beta u^2 - (5 + \beta)(2 + u)v + (5 + \beta)v^2) + z \left(2H^3(-5 - \beta + 3(7 + \beta)v) \right. \right. \end{aligned}$$

$$\begin{aligned}
& + H^2(-3(-1+\beta)uv - 6(5+\beta)z + 8(8+\beta)vz + 6\beta z^2) + H \left(-u^2(-32 + 22u + 63v + \beta(-14 + 12u + 29v)) \right. \\
& - u(21 + 52u + \beta(3 + 20u) - 24v)z + 6(-5 + 7u + 7v)z^2 \Big) + z \left[-5(9 + 5\beta)u^3 - 2(10 + 3\beta)u^2z + 2(5 + \beta)(-1 + v)z^2 \right. \\
& \left. + 3uz(2\beta(-1 + v) + (7 + \beta)z) \right] \Big) \Big\} + \beta \left[-D_1^2 J^4 \left(B(7 + 11\beta)H(H - 2u)v + H \left(-((7 + 11\beta)C(1 + 2u)) + 7(-2 + v)v \right. \right. \right. \\
& \left. \left. \left. + \beta v(-40 - 18u + 29v) \right) z + (-36\beta u^2 + 7H(-2 - 3u + v) + \beta H(-22 + 3u + 29v))z^2 + ((7 + 11\beta)H + 14(-1 + \beta)u) \right. \right. \\
& \left. \left. z^3 \right) + 2D_1 H J^2 v \left[2A(-4 + \beta)H J^2 m_b^2 - z \left(4B H s' v (1 + 5\beta + u + 5\beta u - 6u^2 - 11\beta u^2 - (1 + 5\beta)(2 + u)v + (1 + 5\beta)v^2) \right. \right. \\
& \left. \left. + q^2 u \left[BH v (3 + 13u - 3v + \beta(-9 + 13u + 9v)) + z \left(CH (3 + 13u + \beta(-9 + 13u)) + Hv (12 + 20u - 9v + \beta(-36 + 44u \right. \right. \right. \\
& \left. \left. \left. + 27v)) + (-6 + 8Hu + 30u^2 + 26\beta u^2 + 15v - 9v^2 + \beta H(-18 + 40u + 27v))z + (3 - 2u + 9\beta(H + 2u) - 3v)z^2 \right) \right] \right. \\
& \left. + su \left[BH(-H + 2u + \beta(5 + 2u - 5v))v + z \left\{ CH(1 + 5\beta + 2(1 + \beta)u) + Hv(-12u + \beta(24 - 16u - 19v) + v) + (-2 \right. \right. \right. \\
& \left. \left. \left. + 3Hu - 28u^2 + v + v^2 - \beta(16u^2 + H(-10 + 21u + 19v)) \right) z - (H - 2u + \beta(-5 + 18u + 5v))z^2 \right\} \right] + 2s' z [2H^3(-1 + 3v \\
& + \beta(-5 + 21v)) + z(-5(5 + 9\beta)u^3 - 2(3 + 10\beta)u^2z + (-2 + 3u + 21\beta u + 2v)z^2) + H[-u^2(-14 + 12u + 29v + \beta(-32 \\
& + 22u + 63v)) - u(3 + 20u + \beta(21 + 52u - 24v))z + 6(u + \beta(-5 + 7u + 7v))z^2 + 10\beta z^3] + H^2(3(-1 + \beta)uv \\
& + 2z(-3 - 15\beta + 4v + 32\beta v + 3z))] \Big] + 2AH^2 v^2 z \left(H J^2 m_b^2 (A\beta s' + 4(-q^2 + s)u - s'(5H + u + 5z)) + s' z \left\{ (-H + u \right. \right. \\
& \left. \left. - z)[(-1 + \beta)q^2 u + s'(H + 2u + 4\beta u + 5\beta(F + v) + z)](BH v + z(CH + 2H v + Hz + 2uz)) + s[BH(3(1 + \beta)H^2 \right. \right. \\
& \left. \left. - 6(1 + 2\beta)u^2 + 2H(u + 2\beta u))v + z(CH[3 - 2u(1 + 3u) + \beta(3 - 4u(1 + 3u) + 21v^2)] + 3(1 + \beta)H^2 z(-3 + 4v + 3z) \right. \right. \\
& \left. \left. + 2u^2 z(3u - 3\beta u + 2z + 4\beta z) + H\{3(-7 + 5u)v^2 + 9(1 + \beta)v^3 + (5 + 7\beta)u(-2 + z)z + 3(1 + \beta)z^3 + v[15 + \beta[15 \right. \right. \\
& \left. \left. - 7u(4 + u - 3z)] + u(-20 + u + 15z)]\}) \right\} \right] \Big) \Big\} \Theta[D_1(s, s', q^2)], \quad (38)
\end{aligned}$$

$$\begin{aligned}
\rho_{\gamma_\mu \gamma_5}^3(s, s', q^2) &= \int_0^1 du \int_0^{1-u} dv \frac{1}{32\sqrt{3}C^3\pi^2} \\
&\left[- \left((11 + \beta(14 + 11\beta))m_b \langle \bar{s}s \rangle \Theta[L(s, s', q^2)] \right) + 2(1 + \beta - 2\beta^2)C^3 m_b \langle \bar{u}u \rangle \Theta[L'(s, s', q^2)] \right], \quad (39)
\end{aligned}$$

$$\begin{aligned}
\rho_{\gamma_\mu \gamma_5}^4(s, s', q^2) &= \int_0^1 du \int_0^{1-u} dv \int_0^{1-u-v} dz \frac{1}{1024H^5 J^4 \pi^2} \langle 0 | \frac{1}{\pi} \alpha_s G^2 | 0 \rangle \left\{ 2H^5 \left[2(1 + \beta^2)F^2 uz - 2(19 + \beta(12 + 11\beta)) \right. \right. \\
& u^3(v + z) + (1 + \beta)^2 v^2(H + z)(H + 9z) + uv^2(2(1 + \beta^2)(-2 + v) + (35 + 3\beta(14 + 9\beta))z) + F \left(-4(9 + \beta(6 + 5\beta)) \right. \\
& u^2 z + (1 + \beta)^2 v z(H + z) + 2uv(-1 - \beta^2 + [13 + 3\beta(4 + 3\beta)]z) \Big) - 2u^2 v \left(-18 + 19v + 27z + \beta(2(-6 + 7v + 7z) \right. \\
& \left. + \beta(-10 + 11v + 15z)) \right) \Big] + z \left[H^4 v^2 \left(4u(-1 + 2u - 5v) + 2Hv + 2\beta^2[2u(-1 + 2u - 5v) + Hv] \right. \right. \\
& \left. \left. - \beta(14 + 3(-13 + u)u - 26v + 55uv + 12v^2 + 2H(-7 + 6v)) \right) + H^4 v \left(-6(1 + \beta(6 + \beta)) + 2(1 + \beta(45 + \beta))u \right. \right. \\
& \left. \left. + 2(8 + \beta(-3 + 8\beta))u^2 - \left(2 + 50u + \beta(-92 + 201u + \beta(2 + 50u)) \right) v + 16(1 + (-3 + \beta)\beta)v^2 \right) z \right\}
\end{aligned}$$

$$\begin{aligned}
& + H^2 \left[8u^2(1 + 2(-2 + v)v) - 4u(1 + v - 17v^2 + 9v^3) + 4Hv(-1 + v(-3 + 2v)) + 4\beta^2(u^2(2 + 4(-2 + v)v) \right. \\
& \left. - u(1 + v - 17v^2 + 9v^3) + Hv(-1 + v(-3 + 2v)) \right) + \beta \left(u(39 - 3u(1 + 2(-2 + v)v) + v(-369 + 574v - 228v^2)) \right. \\
& \left. - 4H[7 + v(49 + v(-71 + 31v))] \right] z^2 + H^2 \left(\beta(96 + 6u^2 + 8v(-44 + (49 - 18v)v) + u(-157 + 346v - 78v^2)) \right. \\
& \left. + 4(-4u^2 + v(3 + (-6 + v)v) + 2u(1 + v(4 + v))) \right) + 4\beta^2[-4u^2 + v(3 + (-6 + v)v) + 2u(1 + v(4 + v))] z^3 \\
& - 2H[-2u + \beta(-27 + 27H + (59 - 2\beta)u) + \left(5H + \beta(66 + (-39 + 5\beta)H) + 4u + 4\beta(10 + \beta)u \right. \\
& \left. + (8 + \beta(-3 + 8\beta))u^2 \right) v + \left(11H - 26u + \beta(-56 + (17 + 11\beta)H - (115 + 26\beta)u) \right) v^2 + 17\beta v^3] z^4 \\
& + 2H \left(-8(u - 2v)(u - v) + 8v + 8\beta^2(-[(u - 2v)(u - v)] + v) + \beta(-8 + 3u^2 + 12Hv + u(-79 + 174v)) \right) z^5 \\
& + \left(-8(u^2 + 3Hv - 3uv) - 8\beta^2(u^2 + 3Hv - 3uv) + \beta(60H^2 + 3(-79 + u)u + 253uv) \right) z^6 + \left(\beta(-48 + 79u) \right. \\
& \left. - 8(1 + (-5 + \beta)\beta)v \right) z^7 + 12\beta z^8 \Big\} \Theta[D_2(s, s', q^2)], \tag{40}
\end{aligned}$$

$$\rho_{\gamma_\mu \gamma_5}^5(s, s', q^2) = 0, \tag{41}$$

where,

$$D_1(s, s', q^2) = \frac{-H}{J^2} \left(-q^2 u(v + z)A + m_b^2(u + v)(v^2 + vF + Fz) + vz(su - s'A) \right), \tag{42}$$

$$D_2(s, s', q^2) = \frac{-H}{J^2} \left(-q^2 u(v + z)A + m_b^2(u + v)J + vz(su - s'A) \right), \tag{43}$$

$$L = \frac{1}{H^2} \left(-sCu + (-q^2 + s + s')Cu + m_b^2C(u + v) - s'(u^2 + uH + Hv) \right), \tag{44}$$

$$L' = -sCu + (-q^2 + s + s')uB - m_b^2(u + v) + s'(u - u^2 + v - 2uv - v^2), \tag{45}$$

and $\Theta[\dots]$ represents the unit step function. We have used

$$\begin{aligned}
J &= v^2 + vF + Fz, \\
A &= -1 + u + v + z, \\
B &= -1 + u + v, \\
C &= -1 + u, \\
F &= -1 + z, \\
H &= -1 + v. \tag{46}
\end{aligned}$$

- [1] M. Gell-Mann, “A Schematic Model of Baryons and Mesons,” *Phys. Lett.* **8**, 214-215 (1964).
- [2] M. Mattson *et al.* [SELEX], “First Observation of the Doubly Charmed Baryon Ξ_{cc}^+ ,” *Phys. Rev. Lett.* **89**, 112001 (2002), [[arXiv:hep-ex/0208014 \[hep-ex\]](#)].
- [3] A. Ocherashvili *et al.* [SELEX], “Confirmation of the double charm baryon $\Xi_c + (cc)(3520)$ via its decay to p D+ K-,” *Phys. Lett. B* **628**, 18-24 (2005), [[arXiv:hep-ex/0406033 \[hep-ex\]](#)].
- [4] R. Aaij *et al.* [LHCb], “Observation of the doubly charmed baryon Ξ_{cc}^{++} ,” *Phys. Rev. Lett.* **119**, no.11, 112001 (2017), [[arXiv:1707.01621 \[hep-ex\]](#)].
- [5] R. Aaij *et al.* [LHCb], “First Observation of the Doubly Charmed Baryon Decay $\Xi_{cc}^{++} \rightarrow \Xi_c^+ \pi^+$,” *Phys. Rev. Lett.* **121**, no.16, 162002 (2018), [[arXiv:1807.01919 \[hep-ex\]](#)].

- [6] R. Aaij *et al.* [LHCb], “Search for the doubly charmed baryon Ξ_{cc}^+ ,” *Sci. China Phys. Mech. Astron.* **63**, no.2, 221062 (2020), [[arXiv:1909.12273 \[hep-ex\]](#)].
- [7] R. Aaij *et al.* [LHCb], “Search for the doubly charmed baryon Ξ_{cc}^+ in the $\Xi_c^+\pi^-\pi^+$ final state,” *JHEP* **12**, 107 (2021), [[arXiv:2109.07292 \[hep-ex\]](#)].
- [8] R. Aaij *et al.* [LHCb], “Search for the doubly heavy baryons Ω_{bc}^0 and Ξ_{bc}^0 decaying to $\Lambda_c^+\pi^-$ and $\Xi_c^+\pi^-$,” *Chin. Phys. C* **45**, no.9, 093002 (2021), [[arXiv:2104.04759 \[hep-ex\]](#)].
- [9] M. Shekari Tousi and K. Azizi, “Properties of doubly heavy spin-1/2 baryons: The ground and excited states,” *Phys. Rev. D* **109**, no.5, 054005 (2024), [[arXiv:2401.07151 \[hep-ph\]](#)].
- [10] T. M. Aliev, K. Azizi and M. Savci, “Doubly Heavy Spin-1/2 Baryon Spectrum in QCD,” *Nucl. Phys. A* **895**, 59-70 (2012), [[arXiv:1205.2873 \[hep-ph\]](#)].
- [11] T. M. Aliev, K. Azizi and M. Savci, “The masses and residues of doubly heavy spin-3/2 baryons,” *J. Phys. G* **40**, 065003 (2013), [[arXiv:1208.1976 \[hep-ph\]](#)].
- [12] T. M. Aliev and S. Bilmiş, “The mass and residues of radially and orbitally excited doubly heavy baryons in QCD,” *Nucl. Phys. A* **984**, 99-111 (2019), [[arXiv:1904.11279 \[hep-ph\]](#)].
- [13] T. M. Aliev and S. Bilmiş, “Properties of doubly heavy baryons in QCD,” *Turk. J. Phys.* **46**, no.1, 1-26 (2022), [[arXiv:2203.02965 \[hep-ph\]](#)].
- [14] Q. F. Lü, K. L. Wang, L. Y. Xiao and X. H. Zhong, “Mass spectra and radiative transitions of doubly heavy baryons in a relativized quark model,” *Phys. Rev. D* **96**, no.11, 114006 (2017), [[arXiv:1708.04468 \[hep-ph\]](#)].
- [15] Z. G. Wang, “Analysis of the doubly heavy baryon states and pentaquark states with QCD sum rules,” *Eur. Phys. J. C* **78**, no.10, 826 (2018), [[arXiv:1808.09820 \[hep-ph\]](#)].
- [16] D. Ebert, R. N. Faustov, V. O. Galkin and A. P. Martynenko, “Mass spectra of doubly heavy baryons in the relativistic quark model,” *Phys. Rev. D* **66**, 014008 (2002), [[arXiv:hep-ph/0201217 \[hep-ph\]](#)].
- [17] J. R. Zhang and M. Q. Huang, “Doubly heavy baryons in QCD sum rules,” *Phys. Rev. D* **78**, 094007 (2008), [[arXiv:0810.5396 \[hep-ph\]](#)].
- [18] Z. G. Wang, “Analysis of the $\frac{1}{2}^+$ doubly heavy baryon states with QCD sum rules,” *Eur. Phys. J. A* **45**, 267-274 (2010), [[arXiv:1001.4693 \[hep-ph\]](#)].
- [19] S. Rahmani, H. Hassanabadi and H. Sobhani, “Mass and decay properties of double heavy baryons with a phenomenological potential model,” *Eur. Phys. J. C* **80**, no.4, 312 (2020).
- [20] D. L. Yao, “Masses and sigma terms of doubly charmed baryons up to $\mathcal{O}(p^4)$ in manifestly Lorentz-invariant baryon chiral perturbation theory,” *Phys. Rev. D* **97**, no.3, 034012 (2018), [[arXiv:1801.09462 \[hep-ph\]](#)].
- [21] M. Padmanath, “Heavy baryon spectroscopy from lattice QCD,” [[arXiv:1905.10168 \[hep-lat\]](#)].
- [22] Z. S. Brown, W. Detmold, S. Meinel and K. Orginos, “Charmed bottom baryon spectroscopy from lattice QCD,” *Phys. Rev. D* **90**, no.9, 094507 (2014), [[arXiv:1409.0497 \[hep-lat\]](#)].
- [23] Z. Shah and A. K. Rai, “Excited state mass spectra of doubly heavy Ξ baryons,” *Eur. Phys. J. C* **77**, no.2, 129 (2017), [[arXiv:1702.02726 \[hep-ph\]](#)].
- [24] F. Giannuzzi, “Doubly heavy baryons in a Salpeter model with AdS/QCD inspired potential,” *Phys. Rev. D* **79**, 094002 (2009), [[arXiv:0902.4624 \[hep-ph\]](#)].
- [25] Z. Shah, K. Thakkar and A. K. Rai, “Excited State Mass spectra of doubly heavy baryons Ω_{cc} , Ω_{bb} and Ω_{bc} ,” *Eur. Phys. J. C* **76**, no.10, 530 (2016), [[arXiv:1609.03030 \[hep-ph\]](#)].
- [26] A. Valcarce, H. Garcilazo and J. Vijande, “Towards an understanding of heavy baryon spectroscopy,” *Eur. Phys. J. A* **37**, 217-225 (2008), [[arXiv:0807.2973 \[hep-ph\]](#)].
- [27] Z. G. Wang, “Analysis of the $1/2^-$ and $3/2^-$ heavy and doubly heavy baryon states with QCD sum rules,” *Eur. Phys. J. A* **47**, 81 (2011), [[arXiv:1003.2838 \[hep-ph\]](#)].
- [28] T. Yoshida, E. Hiyama, A. Hosaka, M. Oka and K. Sadato, “Spectrum of heavy baryons in the quark model,” *Phys. Rev. D* **92**, no.11, 114029 (2015), [[arXiv:1510.01067 \[hep-ph\]](#)].
- [29] E. Ortiz-Pacheco and R. Bijker, “Masses and radiative decay widths of S- and P-wave singly, doubly, and triply heavy charm and bottom baryons,” *Phys. Rev. D* **108**, no.5, 054014 (2023), [[arXiv:2307.04939 \[hep-ph\]](#)].
- [30] P. C. Qiu and D. L. Yao, “Chiral effective Lagrangian for doubly charmed baryons up to $\mathcal{O}(q^4)$,” *Phys. Rev. D* **103**, no.3, 034006 (2021), [[arXiv:2012.11117 \[hep-ph\]](#)].
- [31] H. I. Alrebdi, T. M. Aliev and K. Şimşek, “Determination of the strong vertices of doubly heavy baryons with pseudoscalar mesons in QCD,” *Phys. Rev. D* **102**, no.7, 074007 (2020), [[arXiv:2008.05098 \[hep-ph\]](#)].
- [32] A. R. Olamaei, K. Azizi and S. Rostami, “Strong vertices of doubly heavy spin-3/2 baryons with light pseudoscalar mesons,” *Chin. Phys. C* **45**, no.11, 113107 (2021), [[arXiv:2102.03852 \[hep-ph\]](#)].
- [33] T. M. Aliev, T. Barakat and K. Şimşek, “Strong $B_{QQ}^*/B_{QQ'}V$ vertices and the radiative decays of $B_{QQ}^* \rightarrow B_{QQ}\gamma$ in the light-cone sum rules,” *Eur. Phys. J. A* **57**, no.5, 160 (2021), [[arXiv:2101.10264 \[hep-ph\]](#)].
- [34] T. M. Aliev and K. Şimşek, “Strong vertices of doubly heavy spin- 3/2 -spin- 1/2 baryons with light mesons in light-cone QCD sum rules,” *Phys. Rev. D* **103**, no.5, 054044 (2021), [[arXiv:2011.07150 \[hep-ph\]](#)].
- [35] S. Rostami, K. Azizi and A. R. Olamaei, “Strong Coupling Constants of the Doubly Heavy Spin-1/2 Baryons with Light Pseudoscalar Mesons,” *Chin. Phys. C* **45**, no.2, 023120 (2021), [[arXiv:2008.12715 \[hep-ph\]](#)].
- [36] A. R. Olamaei, K. Azizi and S. Rostami, “Strong coupling constants of the doubly heavy Ξ_{QQ} Baryons with π Meson,” *Eur. Phys. J. C* **80**, no.7, 613 (2020), [[arXiv:2003.12723 \[hep-ph\]](#)].
- [37] T. M. Aliev and K. Şimşek, “Strong coupling constants of doubly heavy baryons with vector mesons in QCD,”

- Eur. Phys. J. C* **80**, no.10, 976 (2020), [[arXiv:2009.03464 \[hep-ph\]](#)].
- [38] K. Azizi, A. R. Olamaei and S. Rostami, “Strong interaction of doubly heavy spin-3/2 baryons with light vector mesons,” *Eur. Phys. J. C* **80**, no.12, 1196 (2020), [[arXiv:2011.02919 \[hep-ph\]](#)].
- [39] Q. Qin, Y. J. Shi, W. Wang, G. H. Yang, F. S. Yu and R. Zhu, “Inclusive approach to hunt for the beauty-charmed baryons Ξ_{bc} ,” *Phys. Rev. D* **105**, no.3, L031902 (2022), [[arXiv:2108.06716 \[hep-ph\]](#)].
- [40] L. Y. Xiao, Q. F. Lü and S. L. Zhu, “Strong decays of the 1P and 2D doubly charmed states,” *Phys. Rev. D* **97**, no.7, 074005 (2018), [[arXiv:1712.07295 \[hep-ph\]](#)].
- [41] L. Y. Xiao, K. L. Wang, Q. f. Lu, X. H. Zhong and S. L. Zhu, “Strong and radiative decays of the doubly charmed baryons,” *Phys. Rev. D* **96**, no.9, 094005 (2017), [[arXiv:1708.04384 \[hep-ph\]](#)].
- [42] H. S. Li, L. Meng, Z. W. Liu and S. L. Zhu, “Radiative decays of the doubly charmed baryons in chiral perturbation theory,” *Phys. Lett. B* **777**, 169-176 (2018), [[arXiv:1708.03620 \[hep-ph\]](#)].
- [43] Z. X. Zhao, “Weak decays of doubly heavy baryons: the $1/2 \rightarrow 3/2$ case,” *Eur. Phys. J. C* **78**, no.9, 756 (2018), [[arXiv:1805.10878 \[hep-ph\]](#)].
- [44] Z. P. Xing and Z. X. Zhao, “Weak decays of doubly heavy baryons: the FCNC processes,” *Phys. Rev. D* **98**, no.5, 056002 (2018), [[arXiv:1807.03101 \[hep-ph\]](#)].
- [45] L. J. Jiang, B. He and R. H. Li, “Weak decays of doubly heavy baryons: $B_{cc} \rightarrow B_c V$,” *Eur. Phys. J. C* **78**, no.11, 961 (2018), [[arXiv:1810.00541 \[hep-ph\]](#)].
- [46] M. S. Tousi, K. Azizi and H. R. Moshfegh, “Investigation of the semileptonic decay $\Xi_{cc}^{++} \rightarrow \Xi_c + \ell^- \nu \ell$ within QCD sum rules,” *Phys. Rev. D* **110**, no.11, 114001 (2024), [[arXiv:2409.00241 \[hep-ph\]](#)].
- [47] A. S. Gerasimov and A. V. Luchinsky, “Weak decays of doubly heavy baryons: Decays to a system of π mesons,” *Phys. Rev. D* **100**, no.7, 073015 (2019), [[arXiv:1905.11740 \[hep-ph\]](#)].
- [48] W. Wang, F. S. Yu and Z. X. Zhao, “Weak decays of doubly heavy baryons: the $1/2 \rightarrow 1/2$ case,” *Eur. Phys. J. C* **77**, no.11, 781 (2017), [[arXiv:1707.02834 \[hep-ph\]](#)].
- [49] N. Sharma and R. Dhir, “Estimates of W-exchange contributions to Ξ_{cc} decays,” *Phys. Rev. D* **96**, no.11, 113006 (2017), [[arXiv:1709.08217 \[hep-ph\]](#)].
- [50] K. Patel and K. Thakkar, “Transition properties of Doubly Heavy Baryons,” [[arXiv:2408.00335 \[hep-ph\]](#)].
- [51] T. Gutsche, M. A. Ivanov, J. G. Körner and V. E. Lyubovitskij, “Novel ideas in nonleptonic decays of double heavy baryons,” *Particles* **2**, no.2, 339-356 (2019), [[arXiv:1905.06219 \[hep-ph\]](#)].
- [52] T. Gutsche, M. A. Ivanov, J. G. Körner, V. E. Lyubovitskij and Z. Tyulemissov, “Analysis of the semileptonic and nonleptonic two-body decays of the double heavy charm baryon states Ξ_{cc}^{++} , Ξ_{cc}^+ and Ω_{cc}^+ ,” *Phys. Rev. D* **100**, no.11, 114037 (2019), [[arXiv:1911.10785 \[hep-ph\]](#)].
- [53] H. W. Ke, F. Lu, X. H. Liu and X. Q. Li, “Study on $\Xi_{cc} \rightarrow \Xi_c$ and $\Xi_{cc} \rightarrow \Xi'_c$ weak decays in the light-front quark model,” *Eur. Phys. J. C* **80**, no.2, 140 (2020), [[arXiv:1912.01435 \[hep-ph\]](#)].
- [54] H. Y. Cheng, G. Meng, F. Xu and J. Zou, “Two-body weak decays of doubly charmed baryons,” *Phys. Rev. D* **101**, no.3, 034034 (2020), [[arXiv:2001.04553 \[hep-ph\]](#)].
- [55] X. H. Hu, R. H. Li and Z. P. Xing, “A comprehensive analysis of weak transition form factors for doubly heavy baryons in the light front approach,” *Eur. Phys. J. C* **80**, no.4, 320 (2020), [[arXiv:2001.06375 \[hep-ph\]](#)].
- [56] R. H. Li, J. J. Hou, B. He and Y. R. Wang, “Weak Decays of Doubly Heavy Baryons: $B_{cc} \rightarrow BD^{(*)}$,” *Chinese Phys. C* **45** 043108 (2021), [[arXiv:2010.09362 \[hep-ph\]](#)].
- [57] J. J. Han, R. X. Zhang, H. Y. Jiang, Z. J. Xiao and F. S. Yu, “Weak decays of bottom-charm baryons: $B_{bc} \rightarrow B_b P$,” *Eur. Phys. J. C* **81**, no.6, 539 (2021), [[arXiv:2102.00961 \[hep-ph\]](#)].
- [58] W. Wang, Z. P. Xing and J. Xu, “Weak Decays of Doubly Heavy Baryons: SU(3) Analysis,” *Eur. Phys. J. C* **77**, no.11, 800 (2017), [[arXiv:1707.06570 \[hep-ph\]](#)].
- [59] Y. J. Shi, W. Wang, Y. Xing and J. Xu, “Weak Decays of Doubly Heavy Baryons: Multi-body Decay Channels,” *Eur. Phys. J. C* **78**, no.1, 56 (2018), [[arXiv:1712.03830 \[hep-ph\]](#)].
- [60] M. A. Ivanov, J. G. Körner and V. E. Lyubovitskij, “Nonleptonic Decays of Doubly Charmed Baryons,” *Phys. Part. Nucl.* **51**, no.4, 678-685 (2020),
- [61] Y. J. Shi, W. Wang, Z. X. Zhao and U. G. Meißner, “Towards a Heavy Diquark Effective Theory for Weak Decays of Doubly Heavy Baryons,” *Eur. Phys. J. C* **80**, no.5, 398 (2020), [[arXiv:2002.02785 \[hep-ph\]](#)].
- [62] X. H. Hu, Y. L. Shen, W. Wang and Z. X. Zhao, “Weak decays of doubly heavy baryons: “decay constants”,” *Chin. Phys. C* **42**, no.12, 123102 (2018), [[arXiv:1711.10289 \[hep-ph\]](#)].
- [63] R. H. Li and C. D. Lu, “Search for doubly heavy baryon via weak decays,” [[arXiv:1805.09064 \[hep-ph\]](#)].
- [64] Y. J. Shi, W. Wang and Z. X. Zhao, “QCD Sum Rules Analysis of Weak Decays of Doubly-Heavy Baryons,” *Eur. Phys. J. C* **80**, no.6, 568 (2020), [[arXiv:1902.01092 \[hep-ph\]](#)].
- [65] Y. J. Shi, Y. Xing and Z. X. Zhao, “Light-cone sum rules analysis of $\Xi_{QQ'q} \rightarrow \Lambda_{Q'} \pi$ weak decays,” *Eur. Phys. J. C* **79**, no.6, 501 (2019), [[arXiv:1903.03921 \[hep-ph\]](#)].
- [66] Q. A. Zhang, “Weak Decays of Doubly Heavy Baryons: W-Exchange,” *Eur. Phys. J. C* **78**, no.12, 1024 (2018), [[arXiv:1811.02199 \[hep-ph\]](#)].
- [67] T. Gutsche, M. A. Ivanov, J. G. Körner and V. E. Lyubovitskij, “Decay chain information on the newly discovered double charm baryon state Ξ_{cc}^{++} ,” *Phys. Rev. D* **96**, no.5, 054013 (2017), [[arXiv:1708.00703 \[hep-ph\]](#)].
- [68] T. Gutsche, M. A. Ivanov, J. G. Körner, V. E. Lyubovitskij and Z. Tyulemissov, “Ab initio three-loop calculation of the W-exchange contribution to nonleptonic decays of double charm baryons,” *Phys. Rev. D* **99**, no.5, 056013 (2019), [[arXiv:1812.09212 \[hep-ph\]](#)].

- [69] U. Özdem, “Magnetic moments of doubly heavy baryons in light-cone QCD,” *J. Phys. G* **46**, no.3, 035003 (2019), [[arXiv:1804.10921 \[hep-ph\]](#)].
- [70] U. Özdem, “Magnetic dipole moments of the spin- $\frac{3}{2}$ doubly heavy baryons,” *Eur. Phys. J. A* **56**, no.2, 34 (2020), [[arXiv:1906.08353 \[hep-ph\]](#)].
- [71] A. V. Berezhnoy, A. K. Likhoded and A. V. Luchinsky, “Doubly heavy baryons at the LHC,” *Phys. Rev. D* **98**, no.11, 113004 (2018), [[arXiv:1809.10058 \[hep-ph\]](#)].
- [72] T. M. Aliev, K. Azizi and M. Savci, “Mixing angle of doubly heavy baryons in QCD,” *Phys. Lett. B* **715**, 149-151 (2012), [[arXiv:1205.6320 \[hep-ph\]](#)].
- [73] M. A. Shifman, A. I. Vainshtein and V. I. Zakharov, “QCD and Resonance Physics. Theoretical Foundations,” *Nucl. Phys. B* **147**, 385-447 (1979).
- [74] M. A. Shifman, A. I. Vainshtein and V. I. Zakharov, “QCD and Resonance Physics: Applications,” *Nucl. Phys. B* **147**, 448-518 (1979).
- [75] T. M. Aliev, K. Azizi and M. Savci, “Analysis of the $\Lambda_b \rightarrow \Lambda \ell^+ \ell^-$ decay in QCD,” *Phys. Rev. D* **81**, 056006 (2010), [[arXiv:1001.0227 \[hep-ph\]](#)].
- [76] T. M. Aliev, K. Azizi and A. Ozpineci, “Radiative Decays of the Heavy Flavored Baryons in Light Cone QCD Sum Rules,” *Phys. Rev. D* **79**, 056005 (2009), [[arXiv:0901.0076 \[hep-ph\]](#)].
- [77] S. S. Agaev, K. Azizi and H. Sundu, “Strong $Z_c^+(3900) \rightarrow J/\psi \pi^+; \eta_c \rho^+$ decays in QCD,” *Phys. Rev. D* **93**, no.7, 074002 (2016), [[arXiv:1601.03847 \[hep-ph\]](#)].
- [78] K. Azizi, Y. Sarac and H. Sundu, “Analysis of $P_c^+(4380)$ and $P_c^+(4450)$ as pentaquark states in the molecular picture with QCD sum rules,” *Phys. Rev. D* **95**, no.9, 094016 (2017), [[arXiv:1612.07479 \[hep-ph\]](#)].
- [79] Y. M. Wang, H. Zou, Z. T. Wei, X. Q. Li and C. D. Lu, “The Transition form-factors for semi-leptonic weak decays of J / psi in QCD sum rules,” *Eur. Phys. J. C* **54**, 107-121 (2008), [[arXiv:0707.1138 \[hep-ph\]](#)].
- [80] K. Azizi and J. Y. Süngü, “Semileptonic $\Lambda_b \rightarrow \Lambda_c \ell \bar{\nu}_\ell$ Transition in Full QCD,” *Phys. Rev. D* **97**, no.7, 074007 (2018), [[arXiv:1803.02085 \[hep-ph\]](#)].
- [81] T. M. Aliev, K. Azizi and A. Ozpineci, “Semileptonic $B(s) \rightarrow D(sJ)(2460)l \bar{\nu}_l$ decay in QCD,” *Eur. Phys. J. C* **51**, 593-599 (2007), [[arXiv:hep-ph/0608264 \[hep-ph\]](#)].
- [82] T. M. Aliev, K. Azizi and M. Savci, “Strong coupling constants of light pseudoscalar mesons with heavy baryons in QCD,” *Phys. Lett. B* **696**, 220-226 (2011), [[arXiv:1009.3658 \[hep-ph\]](#)].
- [83] S. Agaev, K. Azizi and H. Sundu, “Four-quark exotic mesons,” *Turk. J. Phys.* **44**, no.2, 95-173 (2020), [[arXiv:2004.12079 \[hep-ph\]](#)].
- [84] K. Azizi and N. Er, “X (3872): propagating in a dense medium,” *Nucl. Phys. B* **936**, 151-168 (2018). [[arXiv:1710.02806 \[hep-ph\]](#)].
- [85] P. A. Zyla *et al.* [Particle Data Group], “Review of Particle Physics,” *PTEP* **2020**, no.8, 083C01 (2020).
- [86] Z. G. Wang, “Analysis of the $\frac{1}{2}^\pm$ antitriplet heavy baryon states with QCD sum rules,” *Eur. Phys. J. C* **68**, 479-486 (2010), [[arXiv:1001.1652 \[hep-ph\]](#)].
- [87] Z. G. Wang, “Reanalysis of the heavy baryon states Omega(b), Omega(c), Xi'(b), Xi'(c), Sigma(b) and Sigma(c) with QCD sum rules,” *Phys. Lett. B* **685**, 59-66 (2010), [[arXiv:0912.1648 \[hep-ph\]](#)].
- [88] V. M. Belyaev and B. L. Ioffe, “Determination of Baryon and Baryonic Resonance Masses from QCD Sum Rules. 1. Nonstrange Baryons,” *Sov. Phys. JETP* **56**, 493-501 (1982) ITEP-59-1982.
- [89] V. M. Belyaev and B. L. Ioffe, “Determination of the baryon mass and baryon resonances from the quantum-chromodynamics sum rule. Strange baryons,” *Sov. Phys. JETP* **57**, 716-721 (1983) ITEP-132-1982.
- [90] B. L. Ioffe, “QCD at low energies,” *Prog. Part. Nucl. Phys.* **56**, 232-277 (2006), [[arXiv:hep-ph/0502148 \[hep-ph\]](#)].
- [91] V. V. Kiselev and A. K. Likhoded, “Baryons with two heavy quarks,” *Phys. Usp.* **45**, 455-506 (2002), [[arXiv:hep-ph/0103169 \[hep-ph\]](#)].
- [92] M. Karliner and J. L. Rosner, “Baryons with two heavy quarks: Masses, production, decays, and detection,” *Phys. Rev. D* **90**, no.9, 094007 (2014), [[arXiv:1408.5877 \[hep-ph\]](#)].